PROCEEDINGS A

royalsocietypublishing.org/journal/rspa

Optimized lattice-based metamaterials for elastostatic cloaking

E. D. Sanders[1], M. A. Aguiló[2] and G. H. Paulino[1]

[1]School of Civil and Environmental Engineering, Georgia Institute of Technology, Atlanta, GA 30332, USA

[2]Simulation and Modeling Sciences, Sandia National Laboratories, PO Box 5800, Albuquerque, NM 87185, USA

GHP, 0000-0002-3493-6857

Research

Check for updates

Cite this article: Sanders ED, Aguiló MA, Paulino GH. 2021 Optimized lattice-based metamaterials for elastostatic cloaking. *Proc. R. Soc. A* **477**: 20210418. https://doi.org/10.1098/rspa.2021.0418

Received: 24 May 2021
Accepted: 3 August 2021

Subject Areas:
mechanical engineering, structural engineering, mechanics

Keywords:
cloaking, optimization, topology optimization

Author for correspondence:
G. H. Paulino
e-mail: paulino@gatech.edu

An optimization-based approach is proposed to design elastostatic cloaking devices in two-dimensional (2D) lattices. Given an elastic lattice with a defect, i.e. a circular or elliptical hole, a small region (cloak) around the hole is designed to hide the effect of the hole on the elastostatic response of the lattice. Inspired by the direct lattice transformation approach to elastostatic cloaking in 2D lattices, the lattice nodal positions in the design region are obtained using a coordinate transformation of the reference (undisturbed) lattice nodes. Subsequently, additional connectivity (i.e. a ground structure) is defined in the design region and the stiffness properties of these elements are optimized to mimic the global stiffness characteristics of the reference lattice. A weighted least-squares objective function is proposed, where the weights have a physical interpretation—they are the design-dependent coefficients of the design lattice stiffness matrix. The formulation leads to a convex objective function that does not require a solution to an additional adjoint system. Optimization-based cloaks are designed considering uniaxial tension in multiple directions and are shown to exhibit approximate elastostatic cloaking, not only when subjected to the boundary conditions they were designed for but also for uniaxial tension in directions not used in design and for shear loading.

1. Introduction

To cloak an object is to make it invisible with respect to some physically observable field. For instance, classical cloaking problems aim to re-direct electromagnetic waves around an object such that the electromagnetic

THE ROYAL SOCIETY PUBLISHING

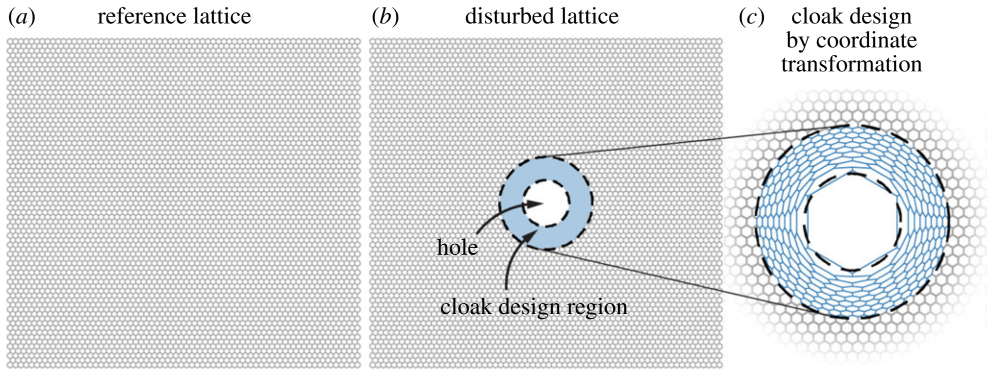

Figure 1. Elastostatic cloak design in 2D lattices: (*a*) reference lattice; (*b*) lattice with a prescribed circular hole surrounded by a region in which a cloak should be designed; (*c*) lattice in which the cloak geometry is defined by a coordinate transformation of the reference lattice nodes. (Online version in colour.)

field is undisturbed and the object is effectively made invisible [1,2]. Relying on form invariance of the underlying (hyperbolic) equations, cloaking with respect to physically observable fields such as electromagnetic waves [1–3], acoustic-induced fluid waves [4,5] and quantum mechanical matter waves [6,7] has traditionally been pursued by applying a coordinate transformation to a given material-parameter distribution and then solving an inverse problem to find a microstructure exhibiting such a transformed distribution. Form invariance has also been exploited to design cloaks in fields governed by time-dependent parabolic equations (e.g. thermodynamics, electrical conduction and particle diffusion) [8–10], and, under special conditions, for fields governed by the elastodynamic wave equation [11–15].

In contrast to the problems listed above, in which the cloak is used to manipulate wave propagation, elastostatic cloaking is used to manipulate the displacement, strain and stress fields induced from static boundary conditions, such that a hole, defect or object becomes undetectable within an elastic medium (figure 1). The elliptic equations governing elastostatics are not form-invariant under coordinate transformations [11]; thus, far fewer attempts have been made to achieve elastostatic cloaking [16,17]. Topology optimization has been pursued for elastostatic cloak design [18,19], but a formulation in the discrete setting that is capable of achieving multi-directional elastostatic cloaking devices that mitigate the influence of circular or elliptical holes has not been fully explored.

2. Overview and related work

Given a two-dimensional (2D) reference lattice (figure 1*a*), the goal of elastostatic cloaking is to design a cloak (blue design region in figure 1*b*) around a prescribed defect (hole) so that, under static boundary conditions, the displacement field outside the cloak matches that of the reference lattice. To accomplish this goal, Bückmann *et al.* [17] proposed a direct lattice transformation (DLT) approach in which the coordinates of the reference lattice nodes are modified to avoid the hole via a coordinate transformation (figure 1*c*) and the local stiffnesses of the connecting elements are held constant by choosing the cross-sectional properties appropriately. For problems like electrical or thermal conductivity, in which each lattice element can be described by a single, scalar parameter (i.e. electrical or thermal resistance), a cloak designed via DLT will exhibit perfect cloaking (in a vacuum) as long as the cross-sectional properties needed to achieve the required resistance of the transformed elements are physically viable [9]. While they acknowledge that the DLT idea may not be directly transferable to cloaking in elastic lattices in which multiple, independent scalars are needed to describe the mechanical behaviour of each lattice element,

royalsocietypublishing.org/journal/rspa *Proc. R. Soc. A* **477**: 20210418

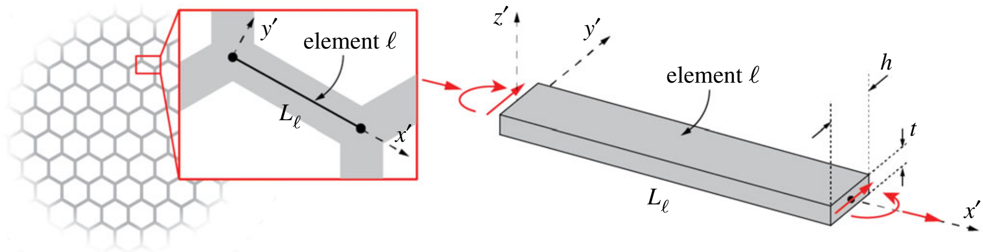

Figure 2. Lattice model: the lattice elements are modelled as Euler–Bernoulli beam elements that also take axial force. The length, height and thickness of element ℓ are L_ℓ, h and t, respectively. In the reference lattice, all elements have the same length, but the length of the lattice elements varies in the design region of the design lattice. (Online version in colour.)

Bückmann *et al.* [17] design the cross-sectional properties of the transformed lattice elements to preserve their axial stiffness. They demonstrate that the approach leads to approximate elastostatic cloaks that perform well for circular holes of varying size, subjected to shear loading and uniaxial compression along two of the lattice's lines of symmetry, with and without lateral support.

It is hypothesized that elastostatic cloaking in 2D lattices can be improved beyond that achieved via the DLT approach. Consider approximating the lattice's mechanical behaviour with a network of Euler–Bernoulli beam elements that also resist axial force. For simplicity, assume that the local stiffness of each lattice element can be mapped exactly from the reference lattice to the transformed lattice (i.e. cross-sectional properties can be found that keep the local stiffness of each lattice element constant in the presence of a change in length). Note that the contribution of each lattice element to the global behaviour of the lattice is dependent not only on its local stiffness but also on its orientation in the network [20]. Thus, even if it were possible to perfectly match the element local stiffnesses to the reference, the global stiffness properties of the transformed lattice would still deviate from those of the reference. Thus, rather than preserving local properties, *global system properties are targeted by designing the nodal connectivity and associated stiffness characteristics in the design region using topology optimization.*

3. Problem setting

Elastostatic cloaking in 2D lattices is pursued in a discrete topology optimization setting where the lattice elements are modelled as Euler–Bernoulli beam elements that can also take axial force (figure 2). The ideas are demonstrated using a hexagonal lattice consisting of elements with rectangular cross-section, but the formulation is not specific to any particular lattice geometry or cross-sectional shape. The height, h, thickness, t, and Young's modulus, E, are the same for all elements in the design lattice; L_ℓ is the length of element ℓ, which may vary in the design region. A full list of nomenclature is provided in appendix A.

(a) Target problem

The specific problem pursued here is outlined in figure 3. The reference lattice contains $N_x \times N_y$ regular hexagons with edge length, L, such that the lattice has width, L_x, and height, L_y. The design lattice is identical to the reference lattice except that an elliptical hole of radius, $R_1(\theta)$, is introduced and enclosed by a circular design region of radius, R_2.

The stiffnesses of the lattice elements are scaled by stiffness parameters, $\mathbf{z} = \{z_\ell\}_{\ell=1}^{N_e}$ and $\widehat{\mathbf{z}} = \{\widehat{z}_\ell\}_{\ell=1}^{\widehat{N}_e}$, for the design and reference lattices, respectively, where N_e is the number of elements in the design lattice and $\widehat{N}_e$ is the number of elements in the reference lattice. The element stiffness matrix of element ℓ is $\mathbf{k}_\ell = z_\ell \mathbf{k}_\ell^0(E,t,h,L_\ell)$ and $\widehat{\mathbf{k}}_\ell = \widehat{z}_\ell \widehat{\mathbf{k}}_\ell^0(E,t,h,L)$, for the design and reference

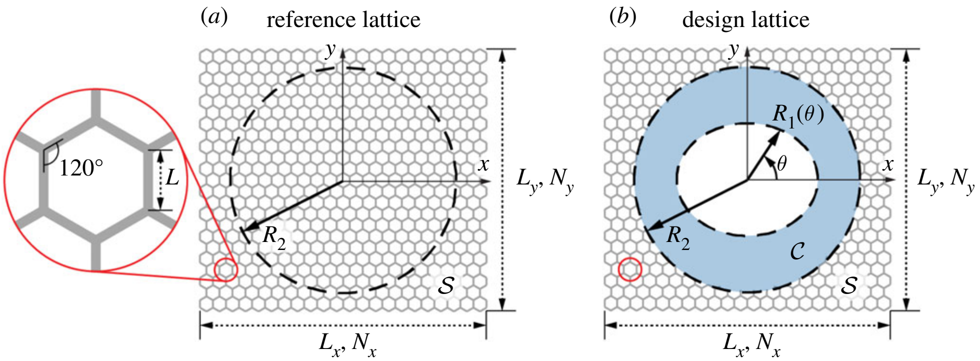

Figure 3. Target problem definition: (*a*) reference lattice and (*b*) design lattice. (Online version in colour.)

lattices, respectively, where $\mathbf{k}_\ell^0$ and $\widehat{\mathbf{k}}_\ell^0$ are the unscaled, constant element stiffness matrices (in global coordinates) of element ℓ (refer to McGuire *et al.* [20]). The set of stiffness parameters for elements with radial coordinates of at least one end node larger than R_2 are members of the surrounding region, $\mathcal{S}$, and are identical in the two lattices, i.e. $z_\ell = \widehat{z}_\ell \ \forall \ell \in \mathcal{S}$. The set of stiffness parameters for elements with radial coordinates of both end nodes between $R_1(\theta)$ and R_2 are members of the design region, $\mathcal{C}$, and will be used as design variables in optimization.[1]

The lattice displacement fields are defined by nodal displacements, $\mathbf{u} = \{u_\ell\}_{\ell=1}^{N_d}$ and $\widehat{\mathbf{u}} = \{\widehat{u}_\ell\}_{\ell=1}^{N_d}$, for the design and reference lattices, respectively, where N_d is the number of degrees of freedom in both the design and reference lattices. The nodal displacements are determined by solving the linear systems, $\mathbf{Ku} = \mathbf{F}$ and $\widehat{\mathbf{K}}\widehat{\mathbf{u}} = \mathbf{F}$, which approximate the elastic response of the design and reference lattices, respectively. The global stiffness matrices, $\mathbf{K}$ and $\widehat{\mathbf{K}}$, of the design and reference lattices are assembled from the element stiffness matrices of each lattice and $\mathbf{F}$ is the vector of applied nodal loads that is the same for both lattices. The set of nodal displacements for nodes with radial coordinates $r > R_2$ are members of the space of nodal displacements in the surrounding region, $\mathcal{S}^u$ and $\widehat{\mathcal{S}}^u$, for the design and reference lattices, respectively.

With the goal of matching the elastostatic response of the design and reference lattices for nodal coordinates with radius $r > R_2$, a cloaking metric,

$$\Delta = \frac{||\mathbf{u}^s - \widehat{\mathbf{u}}^s||_2}{||\widehat{\mathbf{u}}^s||_2}, \tag{3.1}$$

is defined to quantify the cloak's effectiveness [17], where $\mathbf{u}^s = \{u_\ell\}_{\ell \in \mathcal{S}^u}$ and $\widehat{\mathbf{u}}^s = \{\widehat{u}_\ell\}_{\ell \in \widehat{\mathcal{S}}^u}$.

(b) Defining the design space

In a similar spirit to the DLT approach, the design space is defined by first applying a coordinate transformation to the reference lattice's nodal positions, such that they avoid the hole but remain unchanged outside the design region (figure 4*a*,*b*). The particular coordinate transformation considered, illustrated in figure 4*b*, moves points with radial coordinate $\widehat{r} < R_1(\theta)$ in the reference lattice to $R_1(\theta) < r < R_2$ in the design lattice, where $R_1(\theta)$ and R_2 define, respectively, the inner and outer radial coordinates of the elliptical hole and circular cloak along a ray from the origin and

[1] The choice of linear element stiffness scale factors for design variables can be interpreted as material parameters that scale Young's modulus to achieve a multi-material design, or as sizing parameters that scale the element thickness to achieve a variable thickness design. The stiffness matrix is a linear function of both Young's modulus and element thickness (for the case of a rectangular cross-section); other nonlinear design parameters could be targeted, but such choices will have implications for the convexity of the optimization formulation as discussed in §4b.

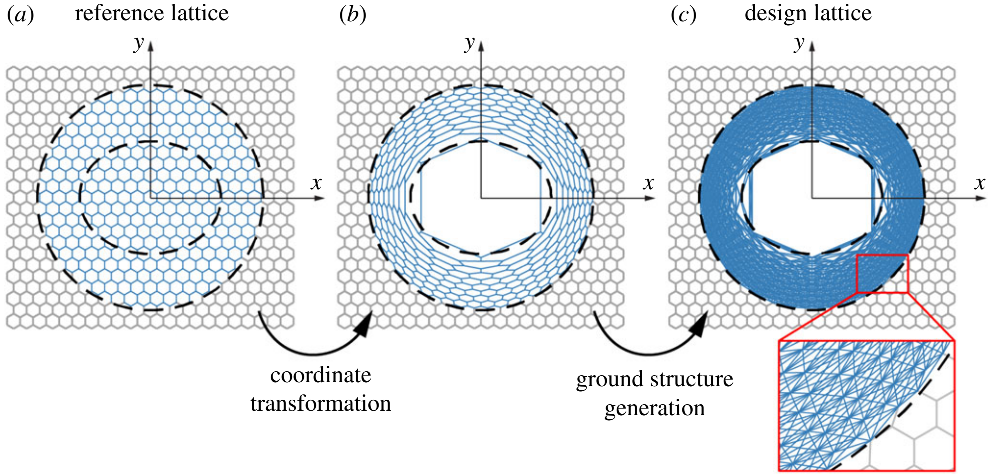

Figure 4. Defining the design space for optimization-based elastostatic cloak design: the reference lattice's nodal positions in (*a*) are modified in (*b*) to avoid a hole using a coordinate transformation that preserves the reference lattice outside of the design region. Subsequently, in (*c*), the design space is enriched by defining a highly redundant ground structure within the design region. (Online version in colour.)

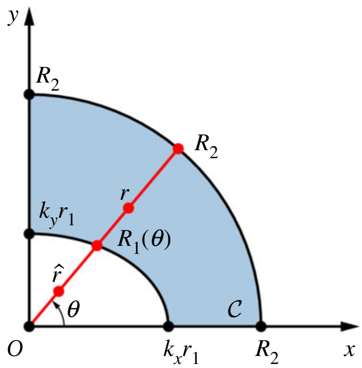

Figure 5. Illustration of the coordinate transformation used to map the reference lattice's nodal positions into the design region in order to avoid the elliptical hole. (Online version in colour.)

passing through $\widehat{r}$ (figure 5). Such a coordinate transformation is described by

$$r = R_1(\theta) + \frac{R_2 - R_1(\theta)}{R_2}\widehat{r}, \quad \text{where } R_1(\theta) = \frac{k_x k_y r_1}{\sqrt{k_y^2 \cos^2(\theta) + k_x^2 \sin^2(\theta)}}, \tag{3.2}$$

where k_x, k_y and r_1 are used to define the semi-major and semi-minor axes of the elliptical hole [21]. Each node of the reference lattice with radial coordinate $r < R_2$ is transformed according to equation (3.2) to define the nodal positions of the design lattice.

To enhance the ability to mimic the global stiffness properties of the reference lattice, the design space is further enriched by defining a ground structure that increases the connectivity in the design region (figure 4*b*,*c*). The ground structures considered here retain all connectivity of the reference lattice and are generated using the ground structure generation tools from the educational code, GRAND [22]. Note that the coordinate transformation stretches the central hexagon radially, and although it ensures that the lattice nodes of this central hexagon avoid the hole, the lattice elements associated with adjacent hexagons may overlap slightly with the hole. These elements are maintained in the design region, but no additional elements are generated within the central hexagon during ground structure generation. Additionally, all

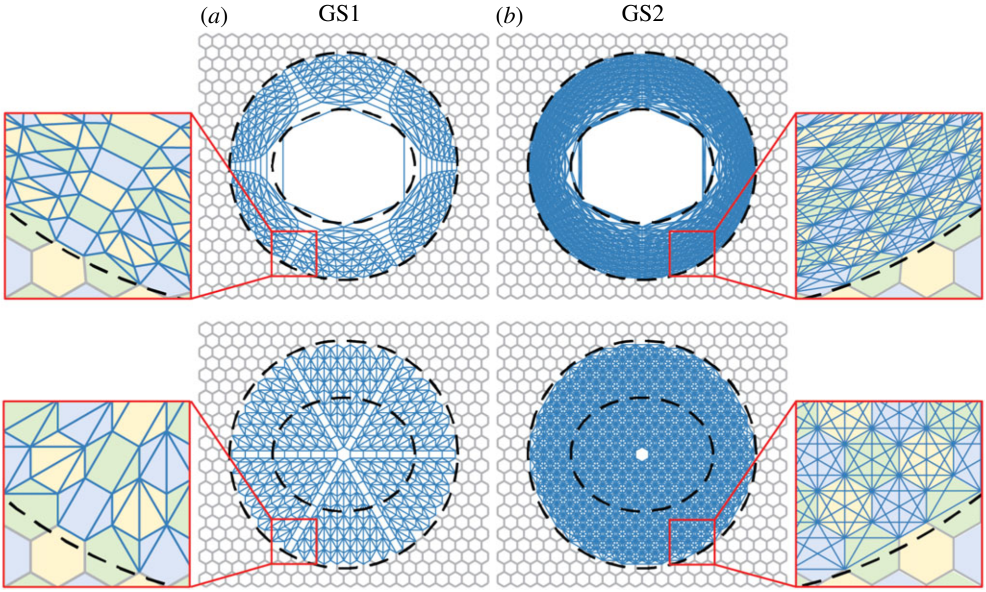

Figure 6. Two ground structures considered in optimization-based elastostatic cloak design: (*a*) GS1 is constructed to achieve the highest connectivity possible, while avoiding crossing members and preserving lattice symmetry with respect to the reference lattice nodal positions; (*b*) GS2 contains level 1 connectivity in which an element is generated between all nodes of each hexagon of the lattice, but not from one hexagon to the next. Connectivity of each ground structure with respect to the reference lattice nodal positions is shown in the second row. Hexagons in the insets are coloured to help visualize the connectivity added with ground structure generation. (Online version in colour.)

ground structures are defined to preserve the symmetries of the reference lattice, although the symmetries do not hold when the coordinate transformation is performed to avoid an elliptical hole (i.e. when $k_x \neq k_y$).

A naive way to select the ground structure is to add a connection between every node in the design region, excluding those that cross the central hexagon. Such a full-level ground structure, as defined by Zegard & Paulino [22], provides the most design freedom; however, a full-level ground structure is extremely dense and will likely lead to designs that are impractical for manufacturing. Instead, two ground structures that are less dense are considered:

(i) GS1 is a ground structure constructed to be as dense as possible, without allowing any crossing members and with hexagonal symmetry preserved (with respect to the nodal coordinates of the reference lattice). Ground structure GS1 is shown in figure 6*a*.

(ii) GS2 is a level 1 ground structure [22] defined to include connectivity between the nodes of each hexagon, but not from one hexagon to the next. This ground structure may still lead to designs that are difficult to manufacture because it is still relatively dense and contains crossing members. Nevertheless, it is considered in an effort to understand the role of increased design freedom. Ground structure GS2 is shown in figure 6*b*.

A number of different ground structures can be defined to achieve the goals of GS1, but numerical experiment indicates that the one selected here is representative of this class of ground structures.

During ground structure generation, if an element centroid's radial coordinate $r > R_2$ that element is removed from the ground structure. To more easily understand the connectivity of the two considered ground structures and to see details of the ground structure near the outer radius of the design region, it is illustrative to look at the ground structure connectivity by considering the nodal positions of the reference lattice, as illustrated at the bottom of figure 6 for the two considered ground structures. Here, the lattice symmetries also become apparent.

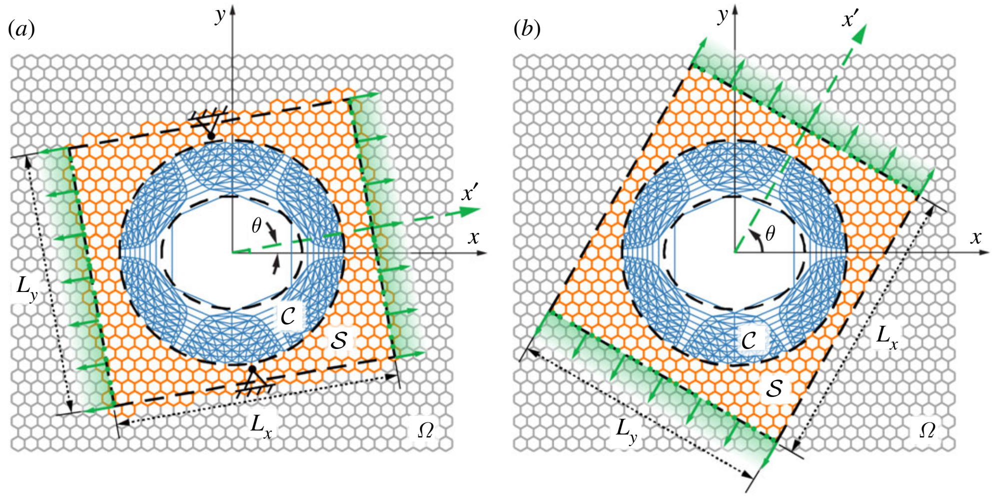

Figure 7. Design lattice embedded in an extended lattice for (*a*) $\theta = 10°$ load angle; (*b*) $\theta = 60°$ load angle. The subset of lattice elements in the surrounding region, $\mathcal{S}$, depends on the load angle, but those in the design region, $\mathcal{C}$, are invariant with respect to the load angle. (Online version in colour.)

(c) Defining the boundary conditions for optimization

An elastostatic cloak should perform well irrespective of the static boundary conditions imposed on the lattice. For example, a low value of Δ should be achieved whether the lattice is subjected to tension, compression, shear, or any other combination of static loads. By considering multiple load cases, not only will the design lattice be less biased towards a specific set of boundary conditions, but multiple load cases will likely also push the global stiffness characteristics of the design lattice closer to those of the reference lattice. For this purpose, various choices and combinations of boundary conditions can be pursued. Perhaps the simplest approach, and the one considered here, is to impose uniaxial tension in several directions to induce different types of loading into each lattice element.

To keep the lattice dimensions, L_x and L_y, constant for each load case, the lattice is embedded in an extended lattice, Ω, as shown in figure 7. Depending on the load angle, θ, a different subset of the extended lattice becomes active. Active lattice elements are those shown in orange in the surrounding region, $\mathcal{S} \subseteq \Omega$, and those shown in blue in the design region, $\mathcal{C} \subseteq \Omega$. The set of lattice elements included in the surrounding region varies depending on the load case, but those in the design region are invariant with respect to the load case.

Lattice elements in the active set are defined as those with centroid falling within the rotated $L_x \times L_y$ bounding box, shown with a black dashed line in figure 7. Depending on the load angle, the bounding box may cut through elements of the extended lattice (refer to the case of $\theta = 10°$ in figure 7*a*). Rather than cutting these lattice elements, a few elements outside the bounding box are included in the active set to avoid partial hexagons. Additionally, for cases in which the loaded edges of the bounding box do not coincide with existing nodes, additional nodes are inserted and loads are applied to these nodes considering the appropriate tributary width. For these cases, which correspond to tensile loads aligned away from the reference lattice's lines of symmetry, the uniaxial loads may not be perfectly equal and opposite. To prevent singularities, two pin supports are added at the centreline of the L_x dimension, as indicated in figure 7*a*. In figure 7*b*, the load angle, $\theta = 60°$, is aligned with a symmetry axis of the reference lattice; thus, no additional nodes are needed for applying the loads and no support conditions are included.[2]

[2]The uniaxial tension loads considered here are self-equilibrated and Tikhonov regularization is used to prevent singularities in the associated system of equations [23,24], as discussed in §5a.

4. Optimization formulation

Optimal design of elastostatic cloaking devices in 2D lattice systems is pursued using an unconstrained optimization statement of the form

$$\min_{\{z_\ell\}_{\ell\in\mathcal{C}}\in[0,1]^N} f(\mathbf{z},\mathbf{u}_1(\mathbf{d}_1),\ldots,\mathbf{u}_{N_\theta}(\mathbf{d}_{N_\theta}))=\sum_{i=1}^{N_\theta}(\widehat{\mathbf{u}}_i-\mathbf{u}_i(\mathbf{d}_i))^T\mathbf{K}_i(\mathbf{d}_i)(\widehat{\mathbf{u}}_i-\mathbf{u}_i(\mathbf{d}_i))$$

$$\text{with } \mathbf{K}_i(\mathbf{d}_i)\mathbf{u}_i(\mathbf{d}_i)=\mathbf{F}_i(\theta_i),\ i=1,\ldots,N_\theta, \tag{4.1}$$

where N_θ load cases (directions) are considered in design. The stiffness parameters of the N_e lattice elements in the extended lattice are stored in $\mathbf{z}=\{z_\ell\}_{\ell=1}^{N_e}$. The subset of lattice elements outside the design region, $\{z_\ell\}_{\ell\in\Omega\setminus\mathcal{C}}$, are assigned the same stiffness parameters as the reference lattice elements. The design variables, $\{z_\ell\}_{\ell\in\mathcal{C}}\in[0,1]^N$, are the subset of stiffness parameters corresponding to the N lattice elements in the design region. The subset of active elements for load case i are denoted, $\mathbf{d}_i=\{z_\ell\}_{\ell\in\mathcal{C}\cup\mathcal{S}_i}$, where $\mathcal{S}_i$ is the space of lattice elements in the surrounding region for load case i. The stiffness matrix and displacement vector of the design lattice for load case i are $\mathbf{K}_i(\mathbf{d}_i)$ and $\mathbf{u}_i(\mathbf{d}_i)$, respectively. The displacement field, $\widehat{\mathbf{u}}_i$, of the reference lattice is determined by the state equations of the reference lattice, $\widehat{\mathbf{K}}_i\widehat{\mathbf{u}}_i=\mathbf{F}_i(\theta_i)$, where $\widehat{\mathbf{K}}_i$ is the stiffness matrix of the reference lattice for load case i. Applied nodal loads for load case i are stored in the vector, $\mathbf{F}_i(\theta_i)$.

The objective function, f, in equation (4.1) is a weighted least-squares function, where the weights are the design-dependent coefficients of the design lattice's stiffness matrix. Weighted least-squares methods are often used when portions of the data should be prioritized more than others [25]. Since cloaking effectiveness is evaluated by only considering the displacements in the surrounding region through the cloaking metric, Δ, one choice of weights could be one that nullifies terms related to displacements that are not in the surrounding region (i.e. an indicator matrix would replace the stiffness matrix in the objective function in equation (4.1)). Based on insights from cloaking in other fields [1,2], it is clear that the properties of the design region play a critical role in achieving effective cloaking and the response in the design region should also be controlled.

By choosing the stiffness coefficients for weights as in equation (4.1), the degrees of freedom in the surrounding region will always be prioritized since the stiffness contributions of the lattice elements in the surrounding region are finite (and fixed). The degrees of freedom in the design region will also be prioritized, likely to a greater extent than those in the surrounding region at the beginning of the optimization when connectivity is dense, and will likely lead to changes in the design variables that cause the global stiffness contribution at each degree of freedom to become closer to that contributing to the associated degree of freedom in the reference lattice. Sparsity of the stiffness matrix leads to many null terms in the least-squares summation, i.e. terms of the form $(\widehat{u}_i-u_i)K_{ij}(\widehat{u}_j-u_j), i\neq j$, when degrees of freedom i and j are not connected in the lattice system. These terms are not as critical in driving the global stiffness of the design lattice towards that of the reference.

Using the stiffness matrix coefficients as weights also endows the objective function with two desirable properties that will be elaborated on in the following two subsections: no solution of an additional adjoint system in computing its sensitivities is needed and the objective function is convex when the stiffness matrix is a linear function of the design variables.

(a) Sensitivity analysis

The adjoint method is used to derive the sensitivities of the objective function, f, in equation (4.1). For simplicity of notation, the dependence on $\mathbf{d}_i=\{z_\ell\}_{\ell\in\mathcal{C}\cup\mathcal{S}_i}$ is dropped in the following derivations.

The state equations of the design lattice, although implicitly enforced in the solution of equation (4.1), serve as partial differential equation (PDE) constraints. The Lagrangian of the associated PDE-constrained optimization problem is

$$\mathcal{L}(\mathbf{z},\mathbf{u}_1,\ldots,\mathbf{u}_{N_\theta},\boldsymbol{\lambda}_1,\ldots,\boldsymbol{\lambda}_{N_\theta}) = \sum_{i=1}^{N_\theta}[(\widehat{\mathbf{u}}_i-\mathbf{u}_i)^T\mathbf{K}_i(\widehat{\mathbf{u}}_i-\mathbf{u}_i)+\boldsymbol{\lambda}_i^T(\mathbf{K}_i\mathbf{u}_i-\mathbf{F}_i(\theta_i))], \tag{4.2}$$

where $\boldsymbol{\lambda}_i$ is the adjoint vector for load case i that can be chosen freely since the second term of the summation in equation (4.2) vanishes owing to equilibrium of the design lattice. Then, the derivative of the objective function with respect to each design variable is

$$\frac{\partial f}{\partial z_\ell} = \frac{\partial \mathcal{L}}{\partial z_\ell} = \sum_{i=1}^{N_\theta}\left[(\widehat{\mathbf{u}}_i-\mathbf{u}_i)^T\frac{\partial \mathbf{K}_i}{\partial z_\ell}(\widehat{\mathbf{u}}_i-\mathbf{u}_i)+\boldsymbol{\lambda}_i^T\frac{\partial \mathbf{K}_i}{\partial z_\ell}\mathbf{u}_i+(-2\mathbf{K}_i\widehat{\mathbf{u}}_i+2\mathbf{K}_i\mathbf{u}_i+\boldsymbol{\lambda}_i^T\mathbf{K}_i)\frac{\partial \mathbf{u}_i}{\partial z_\ell}\right],\ \forall\,\ell\in\mathcal{C}. \tag{4.3}$$

To avoid computing $\partial\mathbf{u}_i/\partial z_\ell$ in the third term of the summation, the adjoint vector is chosen to be

$$\boldsymbol{\lambda}_i = 2(\widehat{\mathbf{u}}_i-\mathbf{u}_i), \tag{4.4}$$

such that the adjoint equation pre-multiplying $\partial\mathbf{u}_i/\partial z_\ell$ in equation (4.3) vanishes. Note that $\boldsymbol{\lambda}_i$ is a function of known quantities and does not require an additional linear solve. With the adjoint vectors known, the derivative of the objective function in equation (4.3) is simplified to be

$$\frac{\partial f}{\partial z_\ell} = \sum_{i=1}^{N_\theta}(\widehat{\mathbf{u}}_i-\mathbf{u}_i(\mathbf{d}_i))^T\mathbf{k}_\ell^0(\widehat{\mathbf{u}}_i+\mathbf{u}_i(\mathbf{d}_i)),\ \forall\,\ell\in\mathcal{C}. \tag{4.5}$$

In equation (4.5), it has been noted that the stiffness matrix of the design lattice can be written as a linear function of the design variables,

$$\mathbf{K}_i = \sum_{\ell\in\mathcal{C}\cup\mathcal{S}_i} z_\ell\mathbf{k}_\ell^0(E,t,h,L_\ell),\quad \text{such that } \frac{\partial \mathbf{K}_i}{\partial z_\ell} = \mathbf{k}_\ell^0,\ \forall\,\ell\in\mathcal{C}\cup\mathcal{S}_i. \tag{4.6}$$

(b) Convexity

To investigate convexity of the objective function, f, its Hessian,

$$\frac{\partial^2 f}{\partial z_\ell\partial z_k} = \frac{\partial}{\partial z_k}\left[\sum_{i=1}^{N_\theta}(\widehat{\mathbf{u}}_i^T\mathbf{k}_\ell^0\widehat{\mathbf{u}}_i+\widehat{\mathbf{u}}_i^T\mathbf{k}_\ell^0\mathbf{u}_i-\mathbf{u}_i^T\mathbf{k}_\ell^0\widehat{\mathbf{u}}_i-\mathbf{u}_i^T\mathbf{k}_\ell^0\mathbf{u}_i)\right], \tag{4.7}$$

is considered. Note that the term in brackets is an expanded form of equation (4.5). The second and third terms of the summation in equation (4.7) cancel out, the first term goes to zero since it is the derivative of a constant and the last term is the second derivative of the well-known structural compliance that is ubiquitous in topology optimization. Owing to the proof of convexity of structural compliance by Svanberg [26], the Hessian of f is positive-definite, and, thus, f is convex. Convexity holds because of the assumption that the stiffness matrix of the design lattice can be written as a linear function of the design variables (see equation (4.6)) and there is a one-to-one mapping between nodes in the reference and design lattices.

5. Details of the numerical implementation

In this section, details related to implementation of the topology optimization formulation for design of elastostatic cloaking devices in 2D lattices are provided. Specifically addressed are Tikhonov regularization to handle low-stiffness elements and self-equilibrated loads, the design variable update scheme, the discrete filtering scheme used to remove thin members during the optimization [24] and the convergence criterion used to stop the iterative optimization algorithm.

(a) Low-stiffness elements and self-equilibrated loading

When the design variables approach zero, the stiffness matrix, $\mathbf{K}_i(\mathbf{d}_i)$, can become ill-conditioned or singular. To avoid ill-conditioning, the state equations are derived by introducing Tikhonov regularization [23], such that the total potential energy of the system for load case i is written as

$$\Pi_i(\mathbf{u}_i(\mathbf{d}_i), \mathbf{d}_i) = \frac{1}{2}\mathbf{u}_i(\mathbf{d}_i)^T\mathbf{K}_i(\mathbf{d}_i)\mathbf{u}_i(\mathbf{d}_i) - \mathbf{F}_i^T\mathbf{u}_i(\mathbf{d}_i) + \frac{\eta}{2}\mathbf{u}_i(\mathbf{d}_i)^T\mathbf{u}_i(\mathbf{d}_i). \tag{5.1}$$

The last term in equation (5.1) is the Tikhonov regularization term and η is the Tikhonov parameter defined as $\eta_0 = 10^{-8}$ multiplied by the mean of the diagonal of $\mathbf{K}_i(\mathbf{d}_i)$. Then according to the principle of minimum potential energy, $\partial\Pi_i/\partial\mathbf{u}_i = 0$ implies that the discretized state equations become $(\mathbf{K}_i\ (\mathbf{d}_i) + \eta\mathbf{I})\mathbf{u}_i\ (\mathbf{d}_i) = \mathbf{F}_i$, where $\mathbf{I}$ is the identity matrix. Tikhonov regularization has also been shown to handle self-equilibrated loads [24], and is used here to regularize the uniaxial tension problems that are specified without support boundary conditions.

(b) Design variable update

The design variables are updated in each optimization iteration using a steepest descent algorithm such that the candidate design variables at iteration $k+1$ are

$$\tilde{z}_\ell^{(k+1)} = z_\ell^{(k)} - \tau^{(k)}\frac{\partial f}{\partial z_\ell^{(k)}}, \ \forall \ell \in \mathcal{C}, \tag{5.2}$$

where inexact line search is used to find the step size, $\tau^{(k)}$, at iteration k [27]. In equation (5.2), $\tilde{z}_\ell^{(k+1)}$ is the value of the design variable associated with lattice element ℓ before the (modified) discrete filter [24] described in the next section is employed.

(c) Discrete filter

A modified discrete filter [24] is employed in each optimization iteration such that members with design variables falling below a given threshold, α_f, are pushed to zero. That is,

$$z_\ell^{(k+1)} = \begin{cases} 0 & \text{if } \dfrac{\tilde{z}_\ell^{(k+1)}}{\max(\{\tilde{z}_\ell\}_{\ell\in\mathcal{C}}^{(k+1)})} < \alpha_f, \\ \tilde{z}_\ell^{(k+1)} & \text{otherwise}, \end{cases} \quad \forall\, \ell \in \mathcal{C}. \tag{5.3}$$

If the filter operation would cause the lattice to become un-equilibrated in a given iteration, the filter operation is skipped in that step. The lattice is said to satisfy equilibrium if the error, $||\mathbf{K}_i\ (\mathbf{d}_i)\mathbf{u}_i\ (\mathbf{d}_i) - \mathbf{F}(\theta_i)||/||\mathbf{F}(\theta_i)\ || \le \mathrm{err}^{\mathrm{tol}}$ (typically $\mathrm{err}^{\mathrm{tol}} = 10^{-4}$).

(d) Convergence criteria

The optimization algorithm is stopped based on stagnation of the cloaking metric, Δ. For load case i, define

$$\Delta_i = \frac{||\mathbf{u}_i^s - \widehat{\mathbf{u}}_i^s||_2}{||\widehat{\mathbf{u}}_i^s||_2}; \tag{5.4}$$

for iteration k, define

$$\delta\Delta_{\max}^{(k)} = \max((\Delta_1^{(k)} - \Delta_1^{(k-1)}), \ldots, (\Delta_{N_\theta}^{(k)} - \Delta_{N_\theta}^{(k-1)})) \tag{5.5}$$

and

$$\delta\Delta_{\min}^{(k)} = \min(|\Delta_1^{(k)} - \Delta_1^{(k-1)}|, \ldots, |\Delta_{N_\theta}^{(k)} - \Delta_{N_\theta}^{(k-1)}|). \tag{5.6}$$

The algorithm is said to have converged when $\delta\Delta_{\max}^{(k)} \ge 10^{-2}$ or when $\delta\Delta_{\min}^{(k)} \le 2\times 10^{-4}$. The first criterion is needed because, although the objective function, f, is convex, Δ is non-convex and may increase over the optimization iterations.

Table 1. Lattice parameters for the elastostatic cloak design studies.

lattice width, L_x	152.04
lattice height, L_y	139.65
reference hexagon edge length, L	4
number of hexagons along lattice width, N_x	22
number of hexagons along lattice height, N_y	12
hole radius, r_1	30
hole semi-major axis parameter, k_x	1 or 1.25
hole semi-minor axis parameter, k_y	1
design region outer radius, R_2	60
Young's modulus, E	100
beam thickness, t	0.8
beam height, h	0.8

6. Elastostatic cloak design studies

The studies included in this section consider the target problem described in figure 3, with unitless lattice parameters provided in table 1. The stiffness parameters in the surrounding region are $z_\ell = \widehat{z}_\ell = 0.8\ \forall \ell \in \Omega \backslash \mathcal{C}$ and the initial value of each design variable is $z_\ell = 0.8\ \forall \ell \in \mathcal{C}$. The discrete filter threshold used during optimization is $\alpha_f = 10^{-4}$. All load cases used in design consider a tensile pressure of $p = 0.8925$ in the positive and negative x' direction as shown in figure 7, applied as nodal loads distributed using an appropriate tributary width. Although only designed for tensile loads, the cloaks are also evaluated in shear. Shear loads are obtained by rotating the tensile loads by 90° counterclockwise. The active portions of the extended lattice for each of the considered load directions are provided in figure 8, where solid green lines indicate loaded edges.

Optimization-based cloaks are designed considering various single- and multi-load-direction cases. The single-load-direction designs are indicated by the angle, θ, for which they were designed. The multi-load-direction designs are indicated according to the following convention:

(i) $\theta_{\text{sym}} = [0°, 30°, 60°, 90°, 120°, 150°]$ includes load directions aligned along the reference lattice's lines of symmetry (shaded cases in figure 8).
(ii) $\theta_{\text{nosym}} = [10°, 45°, 80°, 100°, 135°, 170°]$ includes load directions aligned away from the reference lattice's lines of symmetry (un-shaded cases in figure 8).
(iii) $\theta_{\text{all}} = [0°, 10°, 30°, 45°, 60°, 80°, 90°, 100°, 120°, 135°, 150°, 170°]$ includes all load directions defined in figure 8.

All optimization-based cloaks are designed to minimize the objective function, f, but cloak effectiveness is measured in terms of the cloaking metric, Δ.[3] Using Δ, the optimization-based cloak designs are compared with the 'no cloak' case in which all lattice elements with either of its end nodes within a radius of R_1 are removed and no cloak is designed around the resulting hole. The optimization-based cloak designs are also compared with those designed via a DLT approach similar to the one proposed by Bückmann *et al.* [17]. Recall that the DLT approach defines the nodal positions in the design region by applying the coordinate transformation in equation (3.2) to the nodal positions of the reference lattice, without changing the connectivity. After the coordinate transformation, the cross-sectional properties of each lattice element in the design region are designed so that their axial stiffness is unchanged in the presence of the

[3]Convergence plots for both f and Δ are provided in appendix D for the GS1 optimization-based cloak designs.

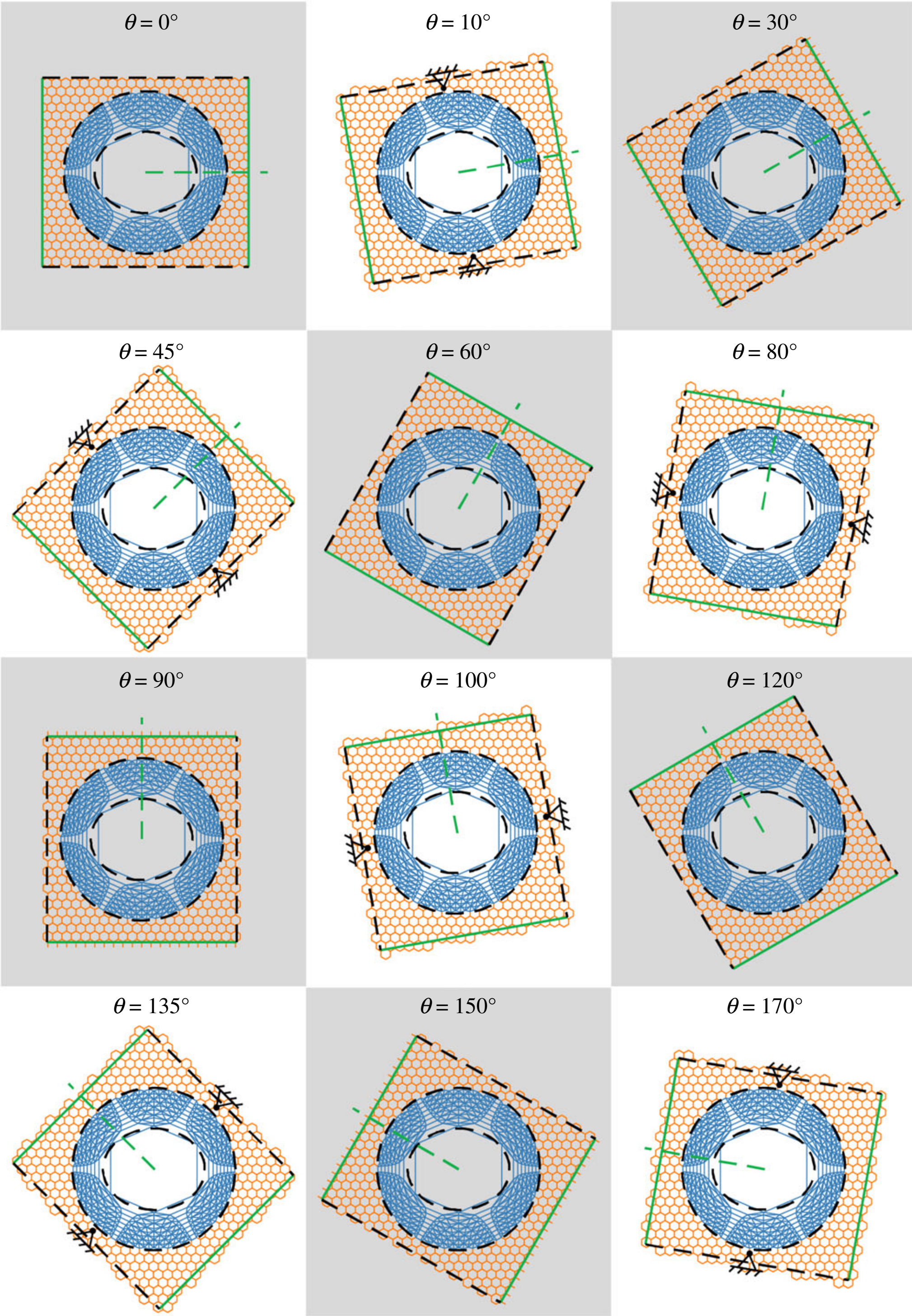

Figure 8. Design lattices considering the elliptical hole ($k_x = 1.25$) for all load directions considered: in all cases, the solid green lines indicate loaded edges and the dashed green lines indicate the direction of uniaxial tension used in design. Shaded cases correspond to loading aligned along a reference lattice line of symmetry. Un-shaded cases correspond to loading aligned away from a reference lattice line of symmetry; in these cases, two pinned supports are included. (Online version in colour.)

Table 2. Number of lattice elements in the design region of the initial ground structures and final designs for selected single- and multi-load-case designs (note that the design region contains 792 lattice elements before ground structure generation).

	initial ground structure	final design ($k_x = 1$)	final design ($k_x = 1.25$)
GS1, $\theta = 0°$	1500	1244	1320
GS1, $\theta = 30°$	1500	1188	1252
GS1, $\theta = 60°$	1500	1244	1248
GS1, $\theta = 90°$	1500	1188	1228
GS1, $\theta_{\rm sym} = [0°, 30°, 60°, 90°, 120°, 150°]$	1500	1140	1238
GS2, $\theta_{\rm sym} = [0°, 30°, 60°, 90°, 120°, 150°]$	3078	1752	2024

element's change in length. Bückmann *et al.* [17] design such axial stiffness by defining a non-uniform cross-section of each lattice element in the design region. Here, a simpler approach is considered in which the stiffness of lattice element $\ell \in \mathcal{C}$ is scaled by L/L_ℓ, where L is the length of each lattice element in the reference lattice and L_ℓ is the length of lattice element ℓ after the coordinate transformation. It is noted that this scaling approach does not observe the box constraints on the design variables used in the optimization problem. In this sense, it provides more design freedom in local element stiffness than the optimization-based approach. A benchmark is provided in appendix B to demonstrate that the Euler–Bernoulli beam model and the axial stiffness transformation considered here provide a DLT cloak with similar performance to that obtained by Bückmann *et al.* [17].

(a) Comparison of single- and multi-load-direction designs

The topology optimization formulation in equation (4.1) is used to design a cloak around a circular hole ($k_x = 1$) and an elliptical hole ($k_x = 1.25$). Using ground structure GS1, designs considering a single load direction in the optimization are compared with designs considering multiple load directions in the optimization. Single-load-case designs are obtained for tensile loading oriented at $\theta = 0°$, $\theta = 30°$, $\theta = 60°$ and $\theta = 90°$. Multi-load-case designs are obtained for tensile loading oriented along the reference lattice's six lines of symmetry, i.e. $\theta_{\rm sym} = [0°, 30°, 60°, 90°, 120°, 150°]$.

The elastostatic cloak designs based on ground structure GS1 and considering the single load directions, $\theta = 0°$ and $\theta = 30°$, are asymmetric, as shown in figure 9*a*,*b*, respectively. The elastostatic cloak design based on ground structure GS1 and considering multiple load cases ($\theta_{\rm sym}$) is shown in figure 10*a*. The symmetrically selected, multiple load cases considered here tend to preserve the symmetries of the reference lattice, although the cloak designed for the elliptical hole is clearly not symmetric.[4] The number of lattice elements in the design region for each of the single-load-case and multi-load-case designs described here are provided in table 2.

The multi-directional performance of each elastostatic cloak design is evaluated by computing the cloaking metric, Δ, for tension and shear loads applied at $\theta = 0°$, $\theta = 30°$, $\theta = 60°$, $\theta = 90°$, $\theta = 120°$ and $\theta = 150°$. In figure 11*a*,*b*, the cloaks designed for the circular ($k_x = 1$) and elliptical ($k_x = 1.25$) holes, respectively, are evaluated in tension. In figure 11*c*,*d*, the cloaks designed for the circular ($k_x = 1$) and elliptical ($k_x = 1.25$) holes, respectively, are evaluated in shear (i.e. for loading conditions not used in design). The effectiveness of the single- and multi-load-case designs considering ground structure GS1 are also compared with the lattice without any cloak around the hole (no cloak), the lattice with the cloak designed using the DLT approach and the lattice with the cloak designed using the multi-load-case, optimization-based approach considering

[4] Appendix C includes a study showing how the single-load-case designs perform when symmetry is enforced on the design variables during optimization.

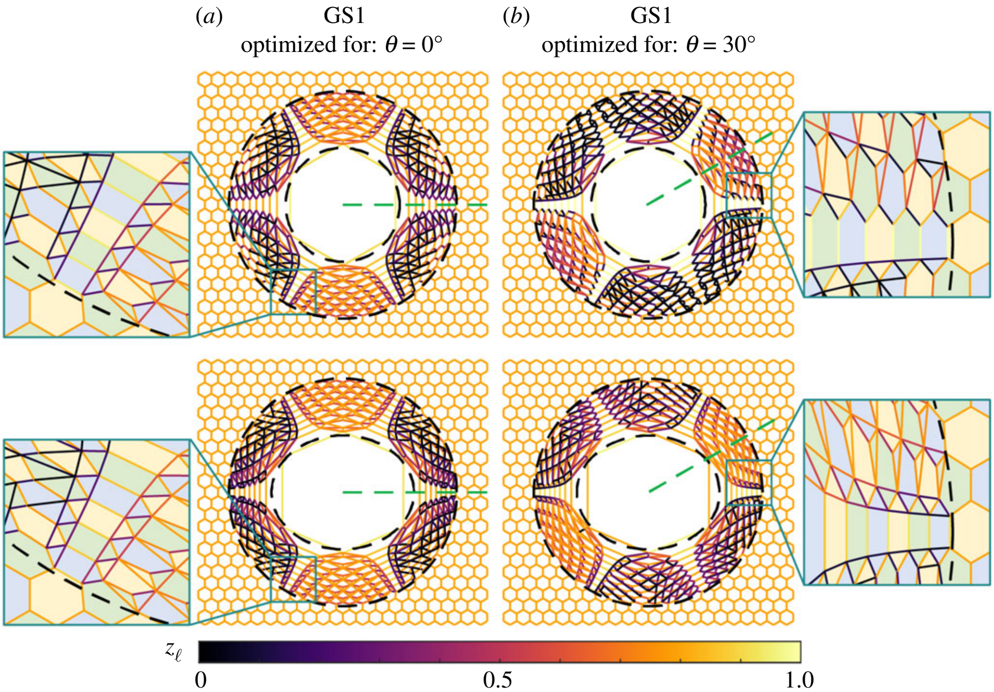

Figure 9. Optimization-based cloak designs based on ground structure GS1 for tensile loads oriented at (*a*) $\theta = 0°$ and (*b*) $\theta = 30°$, as indicated with green dashed lines. The top row is the design for a circular hole ($k_x = 1$) and the bottom row is the design for an elliptical hole ($k_x = 1.25$). Hexagons in the insets are coloured to help visualize the connectivity added with ground structure generation. (Online version in colour.)

ground structure GS2 (designs for the GS2 cloaks are shown in figure 10 and the number of lattice elements in the GS2 design are provided in table 2).

The value of Δ for the single-load-case designs, shown in dashed, coloured lines in figure 11, indicates that the single-load-case designs may be biased towards the load case for which they were designed. In figure 11*a*,*b*, each of the single-load-case designs has the smallest value of Δ for the direction used in design. In some cases, Δ becomes as large as the case with no cloak when loaded in directions not used in design. In other cases (e.g. circular hole, $\theta = 0°$ and $\theta = 60°$ in figure 11*a*), the cloaks obtained from a single load case perform well in all directions.

Figure 11*a*,*b* also shows that the multi-load-case designs (θ_{sym}) are effective in all tensile directions used in design, with relatively constant Δ over load angle. They also outperform the DLT cloak in all load directions considered here. Figure 11*c*,*d* shows that the multi-load-case cloaks also obscure the effect of the hole on the displacement field when loaded in shear, for which they were not designed, and although the DLT cloaks are also effective in shear, the optimization-based cloaks outperform the DLT cloaks to an even greater extent in shear than in tension. The superiority of the multi-load-case, optimization-based cloaks over the DLT cloak in shear may be because the DLT approach focuses on *local axial* stiffness of the lattice elements, whereas the optimization-based approach targets global stiffness characteristics of the lattice as a system. Lastly, because it allows for more freedom during design, the GS2 cloak outperforms the GS1 cloak in all cases, as expected.

The metric, Δ, is a global measure of the cloak's performance. To understand the performance locally, the normalized displacement fields in the x' direction under tensile loading are plotted for the reference, the case of no cloak and the GS1 optimization-based cloak designed for an elliptical hole ($k_x = 1.25$) in figure 12. Similarly, the normalized displacement fields in the y' direction under shear loading are plotted in figure 13. In both cases, it is clear that the cloak obscures the effect of the hole on the displacement fields.

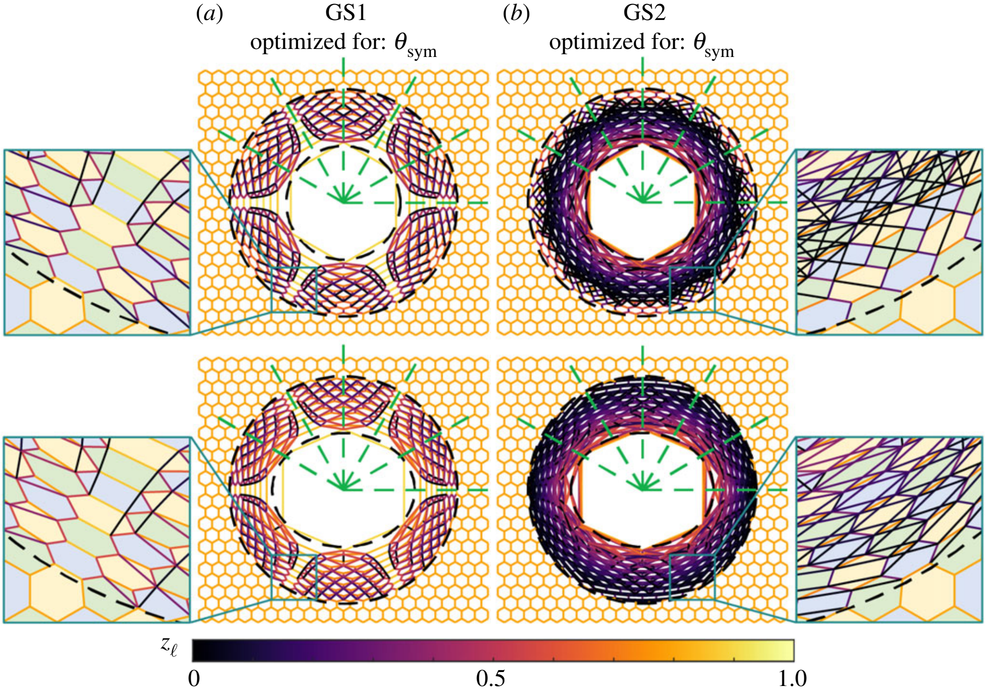

Figure 10. Optimization-based cloak designs based on ground structures (*a*) GS1 and (*b*) GS2 for tensile loads oriented at $\theta_{sym} = [0°, 30°, 60°, 90°, 120°, 150°]$, as indicated with green dashed lines. The top row is the design for a circular hole ($k_x = 1$) and the bottom row is the design for an elliptical hole ($k_x = 1.25$). Hexagons in the insets are coloured to help visualize the connectivity added with ground structure generation.

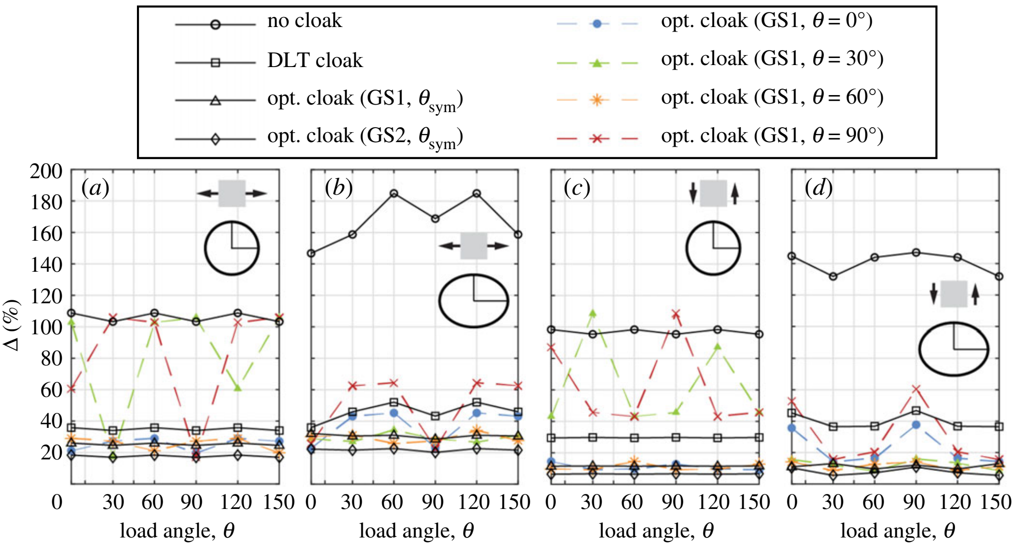

Figure 11. Cloaking metric, Δ, versus load angle, θ, for the no cloak, DLT cloak and optimization-based cloaks: in (*a*,*b*), the cloaks are evaluated under tensile loading for a circular ($k_x = 1$) and an elliptical ($k_x = 1.25$) hole, respectively; in (*c*,*d*), the cloaks are evaluated under shear loading for a circular ($k_x = 1$) and an elliptical ($k_x = 1.25$) hole, respectively. The multi-load-case optimized cloaks were designed considering tensile loads oriented at $\theta_{sym} = [0°, 30°, 60°, 90°, 120°, 150°]$. (Online version in colour.)

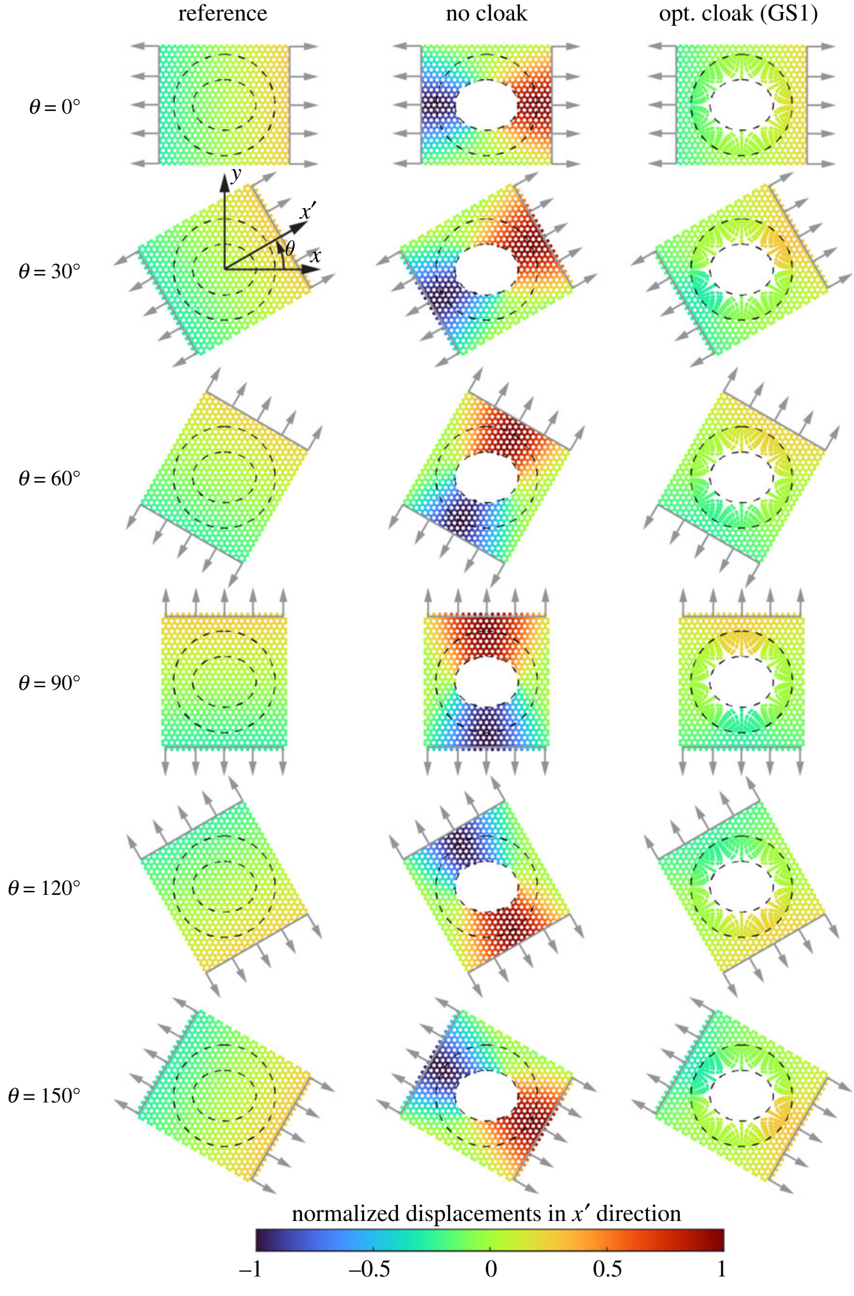

Figure 12. Normalized displacement fields in the x' direction for tensile loading: the left, middle and right columns show, respectively, the displacement fields of the reference lattice, the lattice with no cloak and the lattice with the GS1 optimized cloak designed for an elliptical hole ($k_x = 1.25$) and tensile loads oriented at $\theta_{sym} = [0°, 30°, 60°, 90°, 120°, 150°]$. (Online version in colour.)

(b) Effect of load directions used in design

In the previous sub-section, the load directions considered in multi-load-case design were aligned with the reference lattice's lines of symmetry (i.e. $\theta_{\mathrm{sym}} = [0°, 30°, 60°, 90°, 120°, 150°]$). Here, load directions aligned away from the reference lattice's lines of symmetry are considered in design (i.e. $\theta_{\mathrm{nosym}} = [10°, 45°, 80°, 100°, 135°, 170°]$). Additionally, designs obtained considering θ_{sym} and

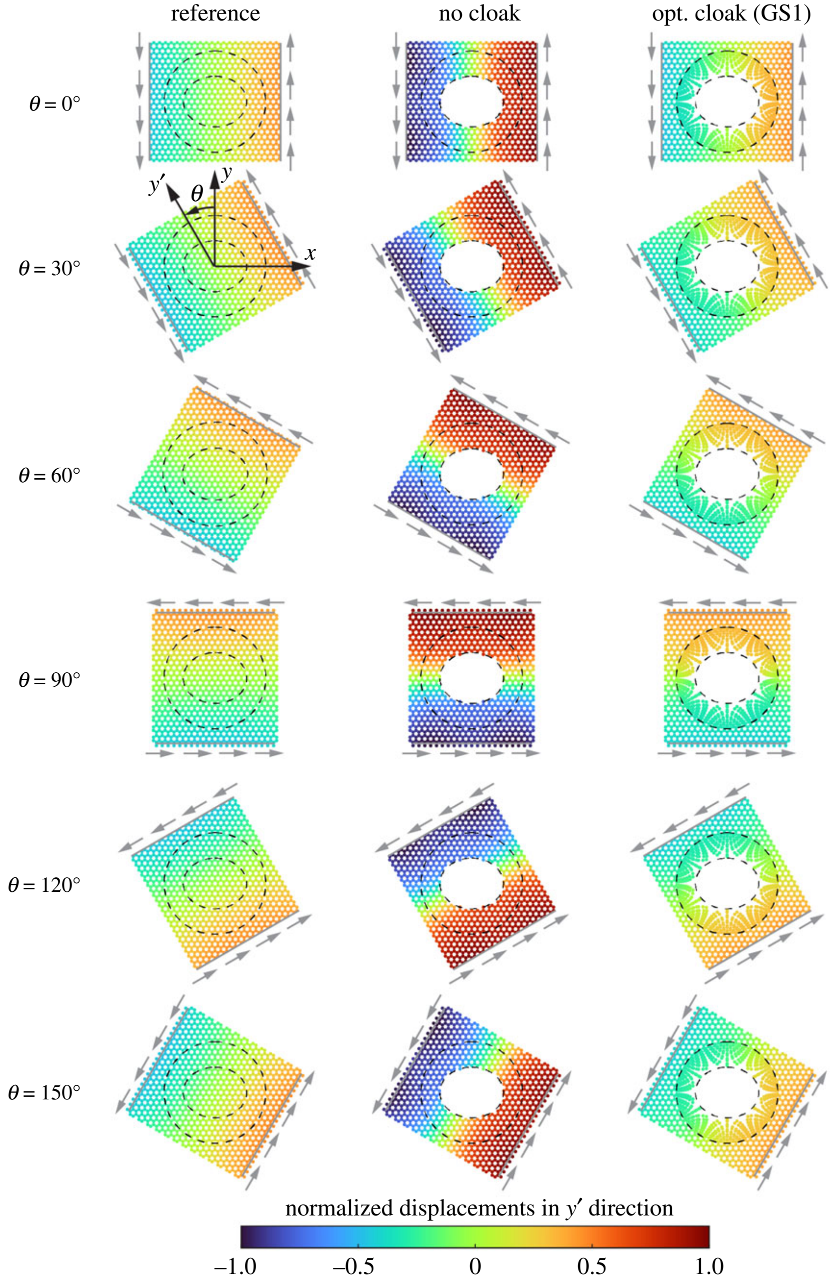

Figure 13. Normalized displacement fields in the y' direction for shear loading: the left, middle and right columns show, respectively, the displacement fields of the reference lattice, the lattice with no cloak and the lattice with the GS1 optimized cloak designed for an elliptical hole ($k_x = 1.25$) and tensile loads oriented at $\theta_{\text{sym}} = [0°, 30°, 60°, 90°, 120°, 150°]$. (Online version in colour.)

θ_{nosym} are evaluated for the directions not used in design and compared with designs obtained considering all 12 load directions simultaneously (i.e. $\theta_{\text{all}} = [0°, 10°, 30°, 45°, 60°, 80°, 90°, 100°, 120°, 135°, 150°, 170°]$). As before, all load cases used in design are tensile loads, but the cloaks are also evaluated for effectiveness in shear.

In the left, middle and right columns of figure 14, the cloaking metric, Δ, is reported for the cloaks designed considering a circular hole and the six tensile load cases aligned along the

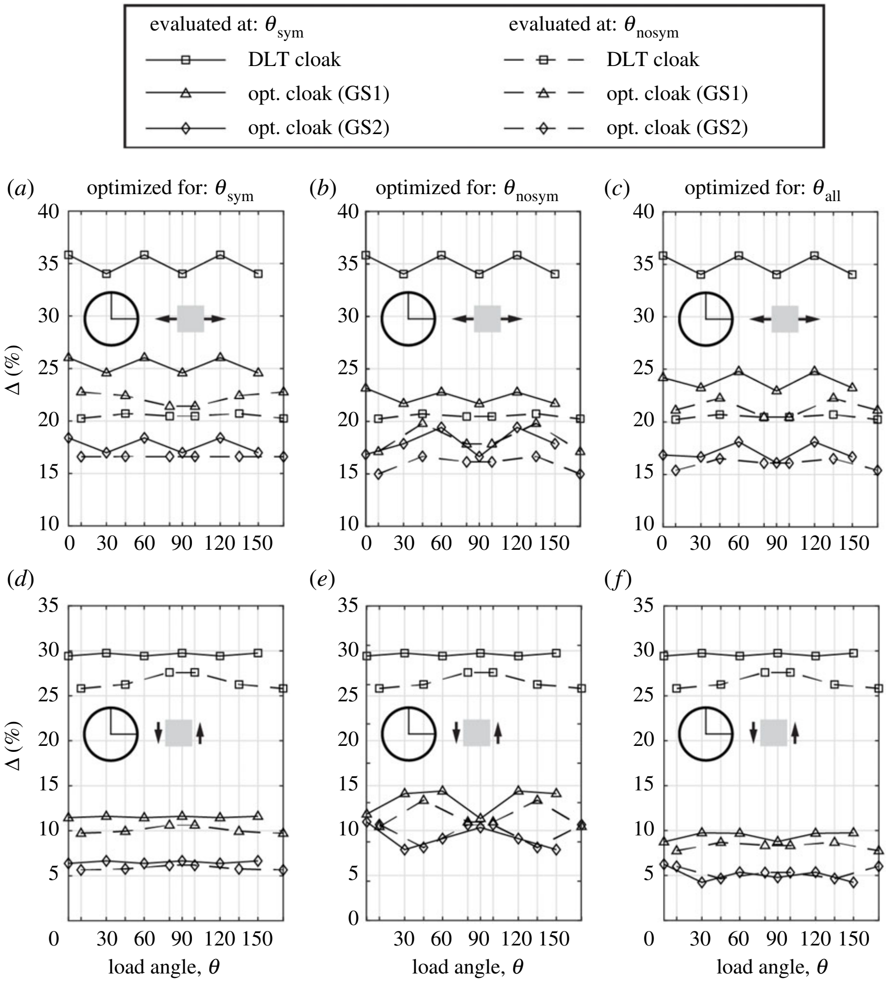

Figure 14. Cloaking metric, Δ, versus load angle, θ, for the DLT cloak and optimization-based cloaks (GS1 and GS2) designed for a circular hole ($k_x = 1$). In (*a–c*), the cloaks are evaluated in tension; in (*d–f*), the cloaks are evaluated in shear. In the left, middle and right columns, Δ is reported for the cloaks designed considering the six tensile load cases aligned along the reference lattice's lines of symmetry (θ_{sym}), the six tensile load cases aligned away from the reference lattice's lines of symmetry (θ_{nosym}) and all 12 tensile load cases (θ_{all}), respectively. Solid and dashed lines indicate Δ evaluated for load directions aligned, respectively, along (i.e. $\theta_{sym} = [0°, 30°, 60°, 90°, 120°, 150°]$) and away from (i.e. $\theta_{nosym} = [10°, 45°, 80°, 100°, 135°, 170°]$) the reference lattice lines of symmetry.

reference lattice's lines of symmetry (θ_{sym}), the six tensile load cases aligned away from the reference lattice's lines of symmetry (θ_{nosym}) and all 12 tensile load cases (θ_{all}), respectively. In the top row Δ is reported for the cloaks evaluated in tension and in the bottom row Δ is reported for the cloaks evaluated in shear. In all plots, Δ is reported for all 12 load directions to understand how these multi-load-case designs behave in directions for which they were not designed. Since the lattice has different stiffnesses along its lines of symmetry than away from its lines of symmetry, solid lines are used to show the response of each lattice when loaded along its lines of symmetry (θ_{sym}) and dashed lines are used to show the response of each lattice when loaded away from its lines of symmetry (θ_{nosym}).

The top row of figure 14 shows that the GS1 cloak performs better in tension for all load directions when designed for tensile loads aligned away from the lattice's lines of symmetry (θ_{nosym}), whereas the GS2 cloak generally performs better in tension in load directions for which it

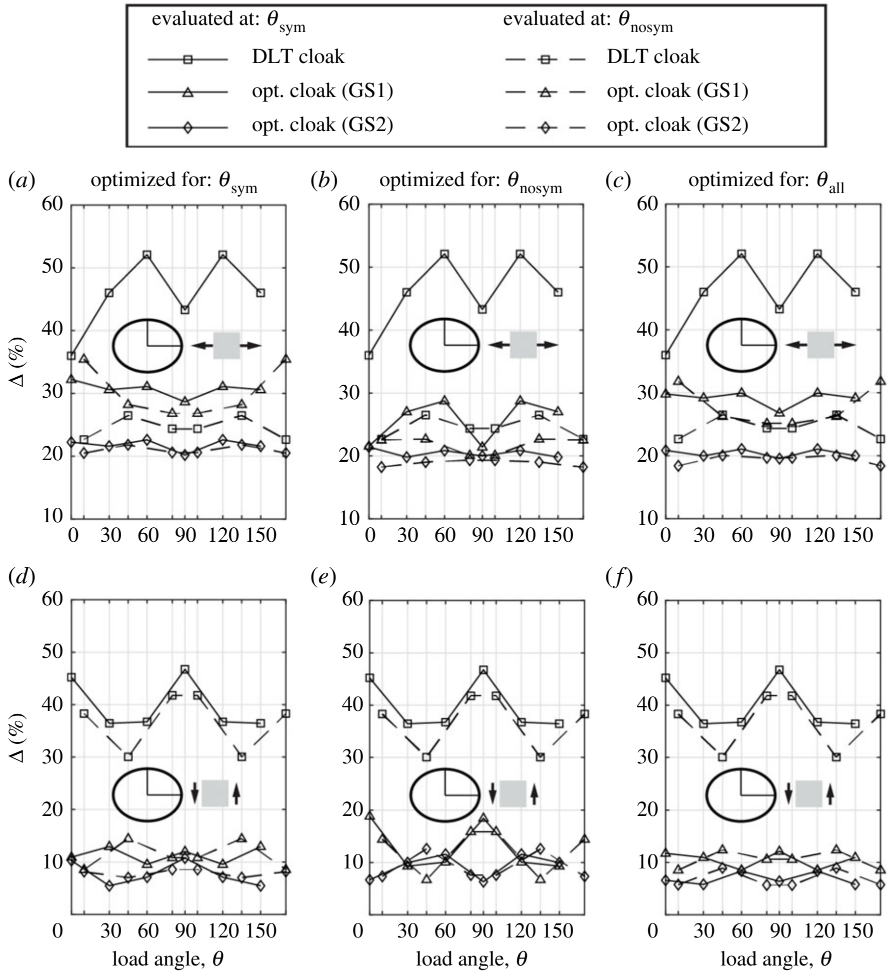

Figure 15. Cloaking metric, Δ, versus load angle, θ, for the DLT cloak and optimization-based cloaks (GS1 and GS2) designed for an elliptical hole ($k_x = 1.25$). In (*a–f*), the cloaks are evaluated in tension; in (*d–f*), the cloaks are evaluated in shear. In the left, middle and right columns, Δ is reported for the cloaks designed considering the six tensile load cases aligned along the reference lattice's lines of symmetry (θ_{sym}), the six tensile load cases aligned away from the reference lattice's lines of symmetry (θ_{nosym}) and all 12 tensile load cases (θ_{all}), respectively. Solid and dashed lines indicate Δ evaluated for load directions aligned, respectively, along (i.e. $\theta = \{0°, 30°, 60°, 90°, 120°, 150°\}$) and away from (i.e. $\theta = \{10°, 45°, 80°, 100°, 135°, 170°\}$) the reference lattice lines of symmetry.

was designed. The GS2 cloak has the most design freedom, and, as expected, always outperforms the GS1 and DLT cloaks. The GS1 cloak always outperforms the DLT cloak in tension for loads aligned along the lattice's lines of symmetry (θ_{sym}, solid lines), but only outperforms the DLT cloak in tension for loads aligned away from the lattice's lines of symmetry (θ_{nosym}, dashed lines) when it is designed for those load cases only (figure 14*b*). When all 12 load cases are considered (θ_{all}, figure 14*c*), the performance of the optimized cloaks is typically somewhere between that of either of the six-load-case results. In general, the optimized cloaks are effective in tension in all directions investigated here. In the case of shear (bottom row of figure 14), the GS1 and GS2 cloaks are always superior to the DLT cloak and the GS2 cloak is always superior to the GS1 cloak. Cloak performance is best in shear when designed for tension in all 12 load directions (θ_{all}, figure 14*e*).

Figure 15 provides a similar study for the case of an elliptical hole and similar trends are observed. The superiority in shear of the GS2 cloak over the GS1 cloak is less clear for the case of an elliptical hole. Nevertheless, all optimized cloaks considered here for an elliptical hole are effective in directions for which they were not designed and are superior to the DLT cloak with the exception of the GS1 cloak when evaluated in tension for directions aligned away from the lattice's lines of symmetry (θ_{nosym}, dashed lines in top row of figure 15*a*,*c*).

7. Conclusion

Approximate elastostatic cloaking devices that hide the effect of a circular or elliptical hole on the displacement field of 2D lattices are designed using topology optimization in a discrete setting in which the lattice elements are modelled using Euler–Bernoulli beam elements that can also take axial force. In an effort to match the global stiffness characteristics of the design lattice to those of the reference (undisturbed) lattice, a weighted least-squares objective function that considers multiple load directions is proposed. This choice of weights nullifies unimportant cross-terms in the least-squares function. Additionally, the selected objective function does not require an extra adjoint solve in computing the sensitivities needed for optimization and is shown to be convex when the stiffness matrix is a linear function of the design variables.

The resulting optimization-based cloaks are shown to outperform elastostatic cloaks designed using the DLT approach [17]. When designed for uniaxial tension applied in multiple directions, the optimization-based cloaks are shown to perform well not only in the directions they were designed for but also in directions they were not designed for. Moreover, although designed only for tensile load cases, the optimization-based cloaks are also shown to perform well in shear and, surprisingly, the superiority of the optimization-based cloaks over the DLT cloaks is even more apparent in shear than in tension. These observations indicate that the optimization-based cloaks do indeed inherit the global stiffness characteristics of the reference lattice.

Although the objective function is convex and, in theory, a global optimum can be found, it is unlikely that perfect cloaking can be achieved with this approach, if at all. Cloaking capabilities in this setting are limited by physical constraints of the design space, e.g. the ground structure connectivity and box constraints on the design variables. Convexity of the current formulation relies on a one-to-one mapping between nodes in the reference and design lattices. Additionally, the nodal positions of the design region, which are determined by the selected coordinate transformation, remain fixed during the optimization. Perhaps improved cloaking could be achieved with a different coordinate transformation (e.g. a cubic coordinate transformation [28]), or by allowing more design freedom in choosing the number and location of nodal positions available in the design region, either *a priori* or as part of the optimization problem. The size and shape of the design region could also be explored and optimized.

As demonstrated in the study comparing single-load-case and multi-load-case designs in §6a, it is apparent that the choice of boundary conditions plays a critical role in mimicking the stiffness characteristics of the reference lattice. One load case is clearly not sufficient, but the multi-load-case study in §6b indicates that too many load cases can also degrade cloaking performance. Additional studies are needed to determine how to best choose the set of boundary conditions considered (e.g. load directions, number of load cases, type of loading conditions, type of support conditions).

Experimental validation of the optimization-based cloaks designed here remains the subject of future work. The GS1 ground structure avoids crossing members in an effort to promote manufacturability. Nevertheless, the geometry of the GS1 cloak is much more complex than that of the cloaks designed by Bückmann *et al.* [17] and manufacturing will be more challenging. Additive manufacturing (AM) provides a promising approach to physically realize the GS1 elastostatic cloaking devices with the design variables interpreted as a linear scale factor on either Young's modulus or beam thickness. The latter interpretation lends itself to most AM technologies that allow for freedom in geometry, but connections between variable-thickness lattice elements may need careful consideration. The former interpretation results in constant thickness over the lattice elements, but requires a multi-material approach or one that can achieve variable stiffness in a continuous range.

Data accessibility. All information needed to reproduce the results is provided in the main text. Additional information can be obtained from the corresponding author upon request.

Authors' contributions. G.H.P. designed the research. M.A.A. and E.D.S. proposed the optimization formulation. E.D.S. performed the numerical implementation and simulations. All authors contributed to writing the manuscript.

Competing interests. The authors have no competing interests.

Funding. We acknowledge Sandia National Laboratories, a multimission laboratory managed and operated by National Technology and Engineering Solutions of Sandia, LLC, a wholly owned subsidiary of Honeywell International, Inc., for the US Department of Energy's National Nuclear Security Administration under contract DE-NA0003525. We also acknowledge the National Science Foundation (NSF) through grant no. 1663244. E.D.S. and G.H.P. acknowledge support from the Raymond Allen Jones Chair at Georgia Institute of Technology. The interpretation of the results of this work is solely that by the authors, and it does not necessarily reflect the views of the sponsors or sponsoring agencies.

Disclaimer. The interpretation of the results of this work is solely that by the authors, and it does not necessarily reflect the views of the sponsors or sponsoring agencies.

Appendix A. Nomenclature

Nomenclature is defined in table 3.

Table 3. Nomenclature.

h	beam height
t	beam thickness
E	Young's modulus
L	length of beam in reference lattice
L_ℓ	length of lattice element ℓ
L_x	lattice width
L_y	lattice height
N_x	number of hexagons along lattice width
N_y	number of hexagons along lattice height
k_x	scale factor for ellipse semi-major axis
k_y	scale factor for ellipse semi-minor axis
$R_1(\theta)$	hole radius
R_2	cloak outer radius
$\mathbf{z}$	vector of design lattice element stiffness scale factors
$\widehat{\mathbf{z}}$	vector of reference lattice element stiffness scale factors
N_e	number of elements in design lattice
$\widehat{N}_e$	number of elements in reference lattice
$\mathbf{k}_\ell^0$	constant element stiffness matrix of element ℓ in design lattice
$\mathbf{k}_\ell$	scaled element stiffness matrix of element ℓ in design lattice
$\widehat{\mathbf{k}}_\ell^0$	constant element stiffness matrix of element ℓ in reference lattice
$\widehat{\mathbf{k}}_\ell$	scaled element stiffness matrix of element ℓ in reference lattice
$\mathcal{S}$	set of elements in surrounding region

(*Continued*.)

Table 3. (*Continued*.)

$\mathcal{C}$	set of elements in design region
$\mathbf{u}$	nodal displacements of design lattice
$\widehat{\mathbf{u}}$	nodal displacements of reference lattice
N_d	number of degrees of freedom in design and reference lattices
$\mathbf{K}$	global stiffness matrix of design lattice
$\widehat{\mathbf{K}}$	global stiffness matrix of reference lattice
$\mathbf{F}$	vector of applied nodal loads
$\mathcal{S}^u$	set of nodal displacements in surrounding region of design lattice
$\widehat{\mathcal{S}}^u$	set of nodal displacements in surrounding region of reference lattice
r	radial coordinate in design lattice
$\widehat{r}$	radial coordinate in reference lattice
θ	polar coordinate
Δ	cloaking metric
$\mathbf{u}^s$	nodal displacement vector for degrees of freedom in surrounding region of design lattice
$\widehat{\mathbf{u}}^s$	nodal displacement vector for degrees of freedom in surrounding region of reference lattice
r_1	un-scaled radius of elliptical hole
Ω	domain of extended lattice
N_θ	number of load cases (directions)
N	number of design variables
$\mathbf{d}_i$	subset of design lattice stiffness scale factors for active elements in load case i
$\mathcal{S}_i$	set of design lattice elements in surrounding region for load case i
$\mathcal{L}$	Lagrangian function
$\boldsymbol{\lambda}_i$	adjoint vector of load case i
$\mathbf{I}$	identity matrix
η	Tikhonov regularization parameter
Π_i	total potential energy of load case i
α_f	discrete filter threshold
$\Delta^{(k)}_{\max}$	maximum change in cloaking metric at iteration k
$\Delta^{(k)}_{\min}$	minimum change in cloaking metric at iteration k

Appendix B. Direct lattice transformation benchmark

Since the lattice systems are modelled differently here from the ones by Bückmann *et al.* [17] and the stiffness transformation is also accomplished differently (see §6), a benchmark is provided to justify comparison between the DLT and optimization-based approaches provided in §6. The benchmark is performed using the target problem described in figure 3 with lattice parameters selected to mimic those in one of the examples by Bückmann *et al.* [17].

The unitless lattice parameters used in the benchmark are outlined in table 4. The model used by Bückmann *et al.* [17] seems to be a 2D, continuum finite-element model. Thus, several discrepancies between it and the beam model used here are noted in table 4. First, the lattice elements in the model by Bückmann *et al.* [17] have variable width: the width is w at the nodes and W at midspan. Additionally, since they presumably use a 2D model, the elements have no

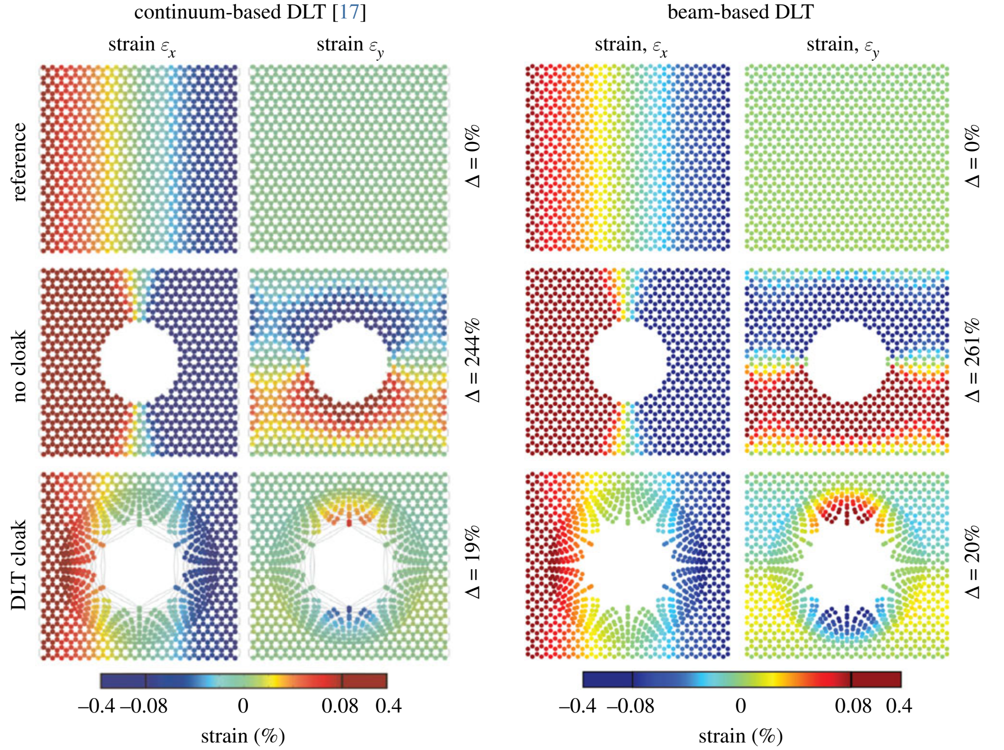

Figure 16. Direct lattice transformation benchmark (no optimization): the left side shows results taken from Bückmann *et al.* [17] and the right side shows the results obtained using the Euler–Bernoulli beam elements and the simplified DLT axial stiffness transformation used here. Strain fields in the horizontal (*x*) and vertical (*y*) directions are provided for the reference lattice, lattice without any cloak and lattice with cloak designed by DLT. The colourbar on the right side is stretched to match that used by Bückmann *et al.* [17] on the left side; that is, all values greater than 20% of the maximum (or less than 20% of the minimum) are mapped to the maximum value (or minimum value) and all other values are scaled by a factor of 5. (Online version in colour.)

thickness. The beam cross-sectional dimensions used here were chosen to be $t = 0.2$ and $h = 0.8$ such that the maximum displacement in the lattice without any cloak most closely matches that observed by Bückmann *et al.* [17]. Note also that, in contrast to the continuum model by Bückmann *et al.* [17], the Euler–Bernoulli beam equations used here neglect the Poisson effect.

To evaluate the effectiveness of the DLT design obtained here and compare it with the results provided by Bückmann *et al.* [17], the $\theta = 0^{\circ}$ lattice is subjected to a uniform, horizontal compressive pressure of $p = 3.3 \times 10^{-5}$, applied as nodal loads on the left and right edges of the lattice, divided equally between the nodes on each edge.[5] Sliding supports are also considered at the top and bottom edges of the lattice. The left side of figure 16 shows the horizontal and vertical strain fields of the reference lattice, lattice with no cloak and lattice with the DLT cloak obtained by Bückmann *et al.* [17] and the right side shows the corresponding fields of the three lattice systems obtained here. Strains in the x and y directions are computed as the displacement in the x or y directions, divided by half of the lattice width, L_x, or height, L_y. The values of Δ reported for each lattice system demonstrate that the approach pursued here is comparable to that used by Bückmann *et al.* [17].

[5]Dividing the pressure equally between the nodes differs from the approach used in the main text, where the pressure is distributed according to tributary width such that the nodes at the corners receive less load than those away from the corners.

Table 4. Lattice parameters for direct lattice transformation benchmark.

	continuum model [17]	beam model
lattice width, L_x	152.04	152.04
lattice height, L_y	139.65	139.65
reference hexagon edge length, L	4	4
number of hexagons along lattice width, N_x	22	22
number of hexagons along lattice height, N_y	12	12
hole radius, r_1	30	30
hole semi-major axis parameter, k_x	1	1
hole semi-minor axis parameter, k_y	1	1
design region outer radius, R_2	60	60
Young's modulus, E	3	3
Poisson's ratio, ν	0.4	—
reference lattice element thickness	—	$t = 0.2$
reference lattice element width	$w = 0.8$, $W = 1$	$h = 0.8$

Appendix C. Enforcing symmetry in single-load-case design

The load directions used to obtain each of the multi-load-case designs in §6 were selected specifically to preserve the symmetries of the reference lattice. It is worth investigating whether enforcing symmetry directly on the design variables and considering a single load case in design is another effective way to achieve multi-directional elastostatic cloaks. The study provided in figure 11 is revisited, with symmetry enforced on the design variables in all cases that consider only a single load direction. To enforce symmetry, all lattice elements in the design region with centroid falling within 30° of the x-axis are taken as design variables and their values are mapped to the remaining lattice elements such that the six rotational and mirror symmetries (with respect to the reference lattice nodal positions) are preserved. The general approach for enforcing symmetry in topology optimization is taken from Almeida *et al.* [29]. The resulting values of Δ are provided in figure 17, where it is demonstrated that enforcing symmetry on the design variables has a negative impact on cloaking performance and causes the single-load-case, optimized cloaks to perform worse than the DLT cloak in all cases.

Appendix D. Convergence of the elastostatic cloaking formulation

Convergence of the objective function, f, is shown for the GS1 cloaks with a circular ($k_x = 1$) and an elliptical ($k_x = 1.25$) hole in figure 18*a*,*b*, respectively, considering single load directions, $\theta = 0°$, $\theta = 30°$, $\theta = 60°$ and $\theta = 90°$, and the three different sets of multiple load directions studied in §6b. The objective function decreases monotonically over the optimization iterations for all of the single- and multi-load-case problems studied here. The objective function values of the single-load-case designs tend to reduce at a faster rate than those of the multi-load-case designs.

In figure 19, convergence of the cloaking metric, Δ, for the GS1 cloaks evaluated in tension is reported for the single-load-case designs. Results for the circular hole ($k_x = 1$) are shown in the left column and results for the elliptical hole ($k_x = 1.25$) are shown in the right column. The cloaking metric, Δ, tends to decrease monotonically over the optimization iterations when evaluated in the load direction for which the cloak was designed; however, Δ may increase over the optimization iterations when considering load directions for which the cloak was not designed.

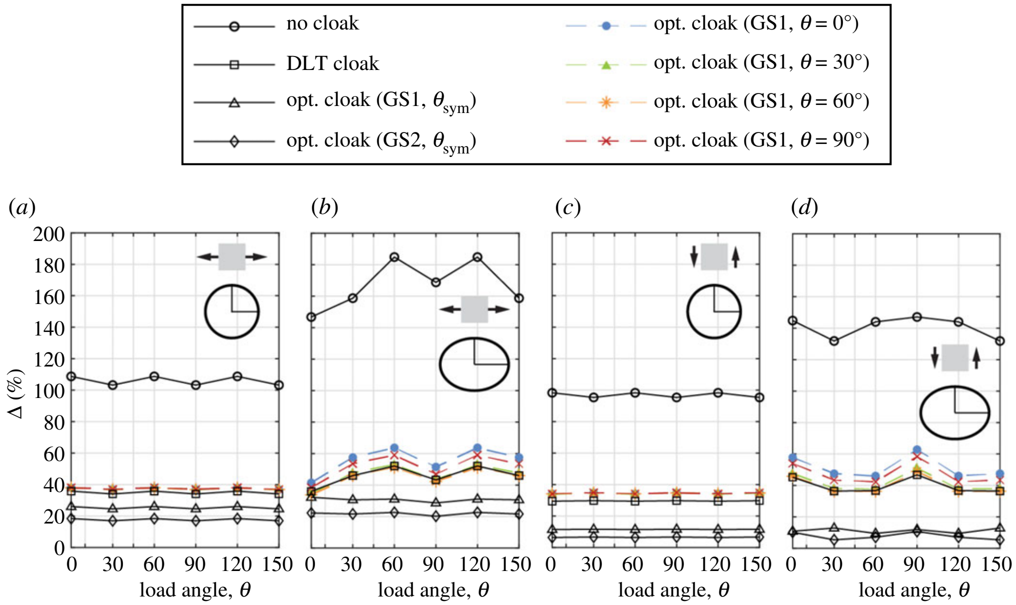

Figure 17. Cloaking metric, Δ, versus load angle, θ, for the no cloak, DLT cloak and optimization-based cloaks: (*a*) and (*b*) evaluate the cloaks under tensile loading for a circular ($k_x = 1$) and an elliptical ($k_x = 1.25$) hole, respectively; (*c*) and (*d*) evaluate the cloaks under shear loading for a circular ($k_x = 1$) and an elliptical ($k_x = 1.25$) hole, respectively. The single-load-case, optimized cloaks were designed with symmetry enforced on the design variables such that the six rotational and mirror symmetries (with respect to the reference lattice nodal positions) are preserved. (Online version in colour.)

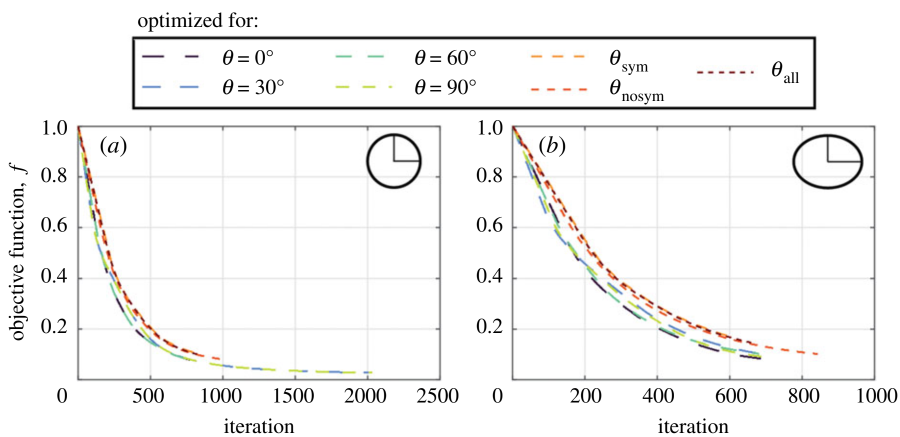

Figure 18. Convergence of the objective function, f, for optimization-based elastostatic cloak designs based on ground structure GS1 and considering single load directions, $\theta = 0°$, $\theta = 30°$, $\theta = 60°$ and $\theta = 90°$, and multiple load directions, $\theta_{sym} = [0°, 30°, 60°, 90°, 120°, 150°]$, $\theta_{nosym} = [10°, 45°, 80°, 100°, 135°, 170°]$, $\theta_{all} = [0°, 10°, 30°, 45°, 60°, 80°, 90°, 100°, 120°, 135°, 150°, 170°]$ for the (*a*) circular hole ($k_x = 1$) and (*b*) elliptical hole ($k_x = 1.25$). In each case, the objective function value is normalized to its value at the initial design. (Online version in colour.)

In figure 20, convergence of the cloaking metric, Δ, for the lattices evaluated in tension is reported for the GS1 multi-load-case designs. Results for the circular hole ($k_x = 1$) are shown in the left column and results for the elliptical hole ($k_x = 1.25$) are shown in the right column. The cloaking metric, Δ, decreases monotonically over the optimization iterations in almost all cases.

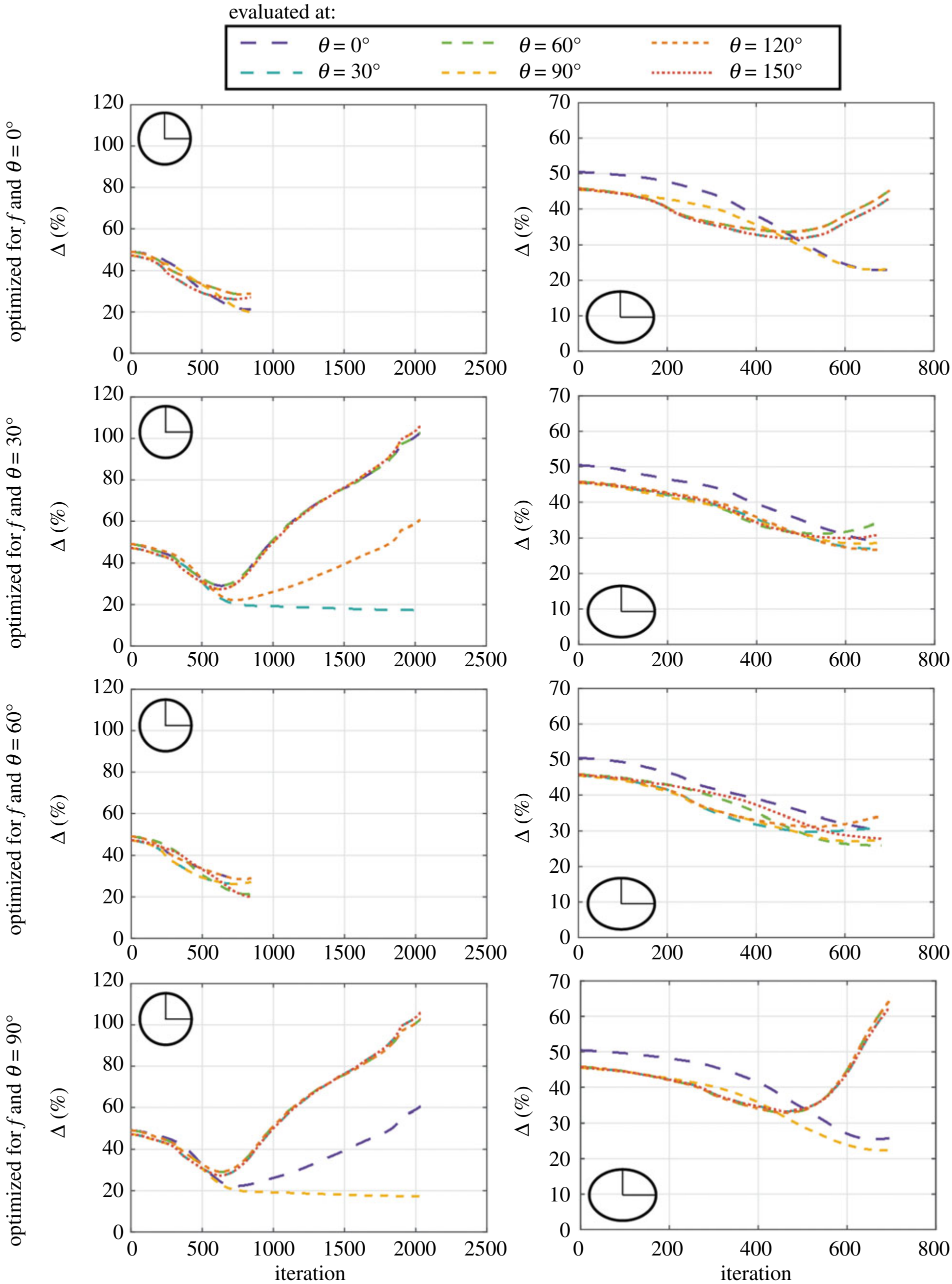

Figure 19. Convergence of the cloaking metric, Δ, for the four different single-load-case, GS1 cloak designs evaluated in directions aligned along the reference lattice's lines of symmetry. The left and right columns show results for the circular ($k_x = 1$) and elliptical ($k_x = 1.25$) holes, respectively. (Online version in colour.)

Small increases in Δ in late iterations are observed for the tensile load cases aligned along the reference lattice's lines of symmetry (θ_{sym}) when the cloak is not designed for these load cases (middle row of figure 20).

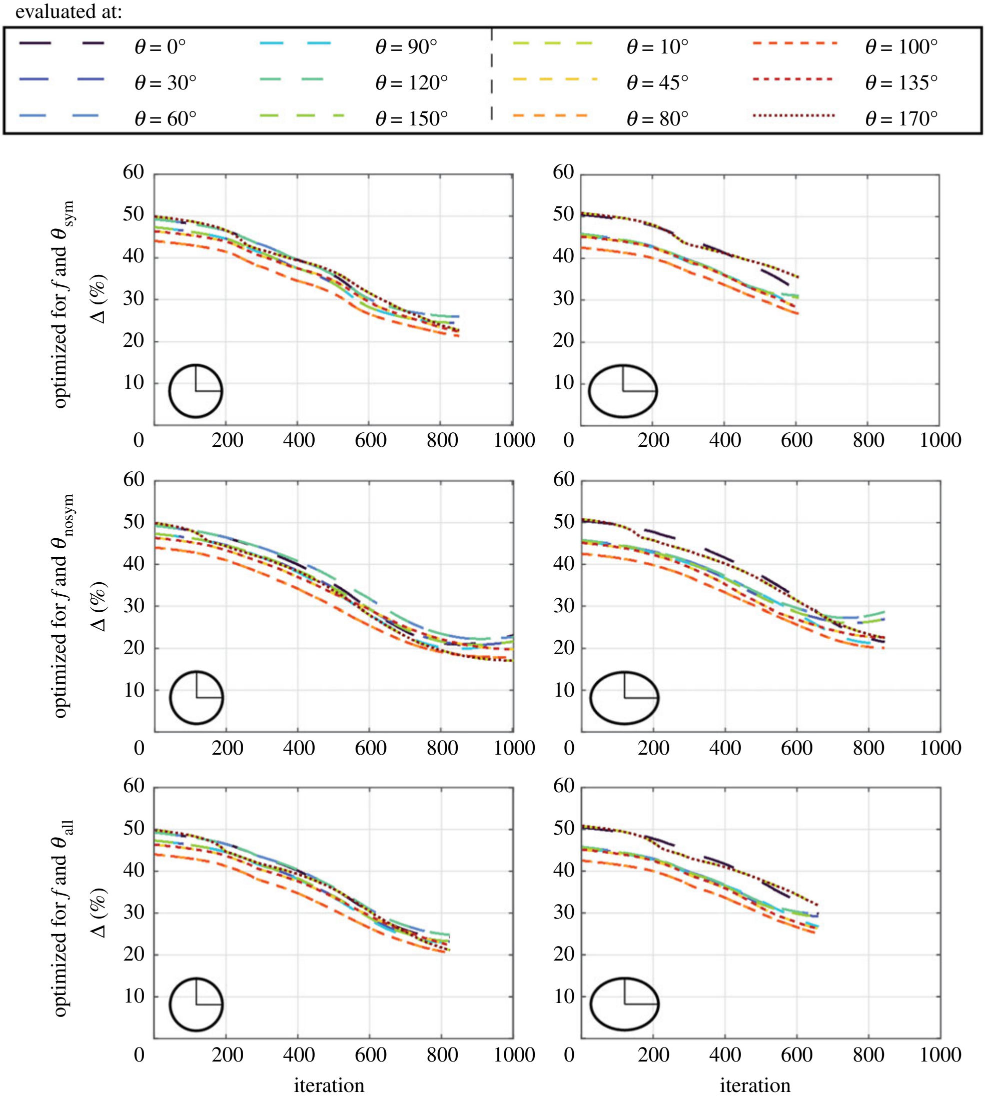

Figure 20. Convergence of the cloaking metric, Δ, for the three different multi-load-case, GS1 cloak designs evaluated in all 12 load directions. The left and right columns show results for the circular ($k_x = 1$) and elliptical ($k_x = 1.25$) holes, respectively. Convergence for cloaks designed considering $\theta_{sym} = [0°, 30°, 60°, 90°, 120°, 150°]$, $\theta_{nosym} = [10°, 45°, 80°, 100°, 135°, 170°]$ and $\theta_{all} = [0°, 10°, 30°, 45°, 60°, 80°, 90°, 100°, 120°, 135°, 150°, 170°]$ are provided in the top, middle and bottom rows, respectively. (Online version in colour.)

References

1. Pendry JB, Schurig D, Smith DR. 2006 Controlling electromagnetic fields. *Science* **312**, 1780–1782. (doi:10.1126/science.1125907)
2. Leonhardt U. 2006 Optical conformal mapping. *Science* **312**, 1777–1780. (doi:10.1126/science.1126493)
3. Schurig D, Mock JJ, Justice BJ, Cummer SA, Pendry JB, Starr AF, Smith DR. 2006 Metamaterial electromagnetic cloak at microwave frequencies. *Science* **314**, 977–980. (doi:10.1126/science.1133628)
4. Farhat M, Enoch S, Guenneau S, Movchan AB. 2008 Broadband cylindrical acoustic cloak for linear surface waves in a fluid. *Phys. Rev. Lett.* **101**, 134501. (doi:10.1103/PhysRevLett.101.134501)

5. Zhang S, Xia C, Fang N. 2011 Broadband acoustic cloak for ultrasound waves. *Phys. Rev. Lett.* **106**, 024301. (doi:10.1103/PhysRevLett.106.024301)
6. Zhang S, Genov DA, Sun C, Zhang X. 2008 Cloaking of matter waves. *Phys. Rev. Lett.* **100**, 123002. (doi:10.1103/PhysRevLett.100.123002)
7. Greenleaf A, Kurylev Y, Lassas M, Uhlmann G. 2008 Approximate quantum cloaking and almost-trapped states. *Phys. Rev. Lett.* **101**, 220404. (doi:10.1103/PhysRevLett.101.220404)
8. Guenneau S, Amra C, Veynante D. 2012 Transformation thermodynamics: cloaking and concentrating heat flux. *Opt. Express* **20**, 8207–8218. (doi:10.1364/OE.20.008207)
9. Schittny R, Kadic M, Guenneau S, Wegener M. 2013 Experiments on transformation thermodynamics: molding the flow of heat. *Phys. Rev. Lett.* **110**, 195901. (doi:10.1103/PhysRevLett.110.195901)
10. Guenneau S, Puvirajesinghe TM. 2013 Fick's second law transformed: one path to cloaking in mass diffusion. *J. R. Soc. Interface* **10**, 20130106. (doi:10.1098/rsif.2013.0106)
11. Milton GW, Briane M, Willis JR. 2006 On cloaking for elasticity and physical equations with a transformation invariant form. *New J. Phys.* **8**, 248. (doi:10.1088/1367-2630/8/10/248)
12. Brun M, Guenneau S, Movchan AB. 2009 Achieving control of in-plane elastic waves. *Appl. Phys. Lett.* **94**, 061903. (doi:10.1063/1.3068491)
13. Stenger N, Wilhelm M, Wegener M. 2012 Experiments on elastic cloaking in thin plates. *Phys. Rev. Lett.* **108**, 014301. (doi:10.1103/PhysRevLett.108.014301)
14. Colquitt DJ, Brun M, Gei M, Movchan AB, Movchan NV, Jones IS. 2014 Transformation elastodynamics and cloaking for flexural waves. *J. Mech. Phys. Solids* **72**, 131–143. (doi:10.1016/j.jmps.2014.07.014)
15. Misseroni D, Colquitt DJ, Movchan AB, Movchan NV, Jones IS. 2016 Cymatics for the cloaking of flexural vibrations in a structured plate. *Sci. Rep.* **6**, 1–11. (doi:10.1038/srep23929)
16. Bückmann T, Thiel M, Kadic M, Schittny R, Wegener M. 2014 An elasto-mechanical unfeelability cloak made of pentamode metamaterials. *Nat. Commun.* **5**, 4130. (doi:10.1038/ncomms5130)
17. Bückmann T, Kadic M, Schittny R, Wegener M. 2015 Mechanical cloak design by direct lattice transformation. *Proc. Natl Acad. Sci. USA* **112**, 4930–4934. (doi:10.1073/pnas.1501240112)
18. Fachinotti VD, Peralta I, Albanesi AE. 2018 Optimization-based design of an elastostatic cloaking device. *Sci. Rep.* **8**, 1–8. (doi:10.1038/s41598-018-28069-7)
19. Álvarez Hostos JC, Fachinotti VD, Peralta I. 2019 Metamaterial for elastostatic cloaking under thermal gradients. *Sci. Rep.* **9**, 1–9. (doi:10.1038/s41598-019-40517-6)
20. McGuire W, Gallagher RH, Ziemian RD. 2000 *Matrix structural analysis*. New York, NY: John Wiley & Sons Inc.
21. Jiang WX, Cui TJ, Yu GX, Lin XQ, Cheng Q, Chin JY. 2008 Arbitrarily elliptical–cylindrical invisible cloaking. *J. Phys. D: Appl. Phys.* **41**, 085504. (doi:10.1088/0022-3727/41/8/085504)
22. Zegard T, Paulino GH. 2014 GRAND—Ground structure based topology optimization for arbitrary 2D domains using MATLAB. *Struct. Multidiscip. Optim.* **50**, 861–882. (doi:10.1007/s00158-014-1085-z)
23. Ben-Israel A, Greville TNE. 2003 *Generalized inverses: theory and applications*, vol. 15. New York, NY: Springer Science & Business Media.
24. Ramos Jr AS, Paulino GH. 2016 Filtering structures out of ground structures—a discrete filtering tool for structural design optimization. *Struct. Multidiscip. Optim.* **54**, 95–116. (doi:10.1007/s00158-015-1390-1)
25. Bard Y. 1974 *Nonlinear parameter estimation*. New York, NY: Academic Press.
26. Svanberg K. 1984 On local and global minima in structural optimization. In *New directions in optimum structural design* (eds E Atrek, RH Gallagher, KM Ragsdell, OC Zienkiewicz). Chichester, UK and New York, NY: John Wiley & Sons.
27. Ascher UM, Greif C. 2011 *A first course on numerical methods*. Philadelphia, PA: SIAM.
28. Kadic M, Wegener M, Nicolet A, Zolla F, Guenneau S, Diatta A. 2020 Elastodynamic behavior of mechanical cloaks designed by direct lattice transformations. *Wave Motion* **92**, 102419. (doi:10.1016/j.wavemoti.2019.102419)
29. Almeida SRM, Paulino GH, Silva ECN. 2010 Layout and material gradation in topology optimization of functionally graded structures: a global-local approach. *Struct. Multidiscip. Optim.* **42**, 855–868. (doi:10.1007/s00158-010-0514-x)